Fibrosis induced by resident macrophages has divergent roles in pancreas inflammatory injury and PDAC

John M. Baer[1], Chong Zuo[1], Liang-I Kang ®[2], Angela Alarcon de la Lastra[1], Nicholas C. Borcherding[2], Brett L. Knolhoff[1], Savannah J. Bogner[1], Yu Zhu[1,3], Liping Yang[4], Jennifer Laurent[4], Mark A. Lewis[1,5], Nan Zhang[2], Ki-Wook Kim ®[2,6], Ryan C. Fields ®[2,7], Wayne M. Yokoyama ®[4], Jason C. Mills ®[5,8,12,13], Li Ding[1,9,10,11], Gwendalyn J. Randolph ®[1,2] & David G. DeNardo ®[1,2,9] ✉

Tissue-resident macrophages (TRMs) are long-lived cells that maintain locally and can be phenotypically distinct from monocyte-derived macrophages. Whether TRMs and monocyte-derived macrophages have district roles under differing pathologies is not understood. Here, we showed that a substantial portion of the macrophages that accumulated during pancreatitis and pancreatic cancer in mice had expanded from TRMs. Pancreas TRMs had an extracellular matrix remodeling phenotype that was important for maintaining tissue homeostasis during inflammation. Loss of TRMs led to exacerbation of severe pancreatitis and death, due to impaired acinar cell survival and recovery. During pancreatitis, TRMs elicited protective effects by triggering the accumulation and activation of fibroblasts, which was necessary for initiating fibrosis as a wound healing response. The same TRM-driven fibrosis, however, drove pancreas cancer pathogenesis and progression. Together, these findings indicate that TRMs play divergent roles in the pathogenesis of pancreatitis and cancer through regulation of stromagenesis.

TRMs are established through embryonic and adult hematopoiesis. At birth, TRMs are derived from embryonic progenitors, but some TRMs are gradually replaced with monocyte-derived cells over time, to varying extents determined at a tissue-specific level[1–9]. 'Closed' TRM populations, such as brain microglia, undergo little monocyte replacement, whereas 'open' TRM populations, such as lung alveolar macrophages, undergo gradual replacement, the extent of which is determined at a tissue-specific level[6,9,10]. On the other hand, short-lived,

monocyte-derived macrophages (MDMs) rely on continual replenishment from circulating monocytes[11,12]. It is understood that both developmental origin and tissue microenvironment offer cues that contribute to macrophage phenotypes[13–15]. TRMs have a variety of roles in maintaining tissue homeostasis, extracellular matrix (ECM) remodeling and inflammation[16]. Across the fat, dermis, heart, lung and mesenteric membranes, it is thought that interstitial TRMs can be subdivided into at least two major subpopulations, LYVE1^{hi}CX$_3$CR1^{lo}MHCII$^{lo/int}$ and LYVE1^{lo}CX$_3$CR1^{hi}MHCII^{hi} cells, with LYVE1^{hi}CX$_3$CR1^{lo}MHCII$^{lo/Int}$ TRMs reported to be involved in ECM remodeling[17–20]. However, it is not fully understood how TRM subsets and MDMs might be uniquely poised to respond to tissue damage or pathologic conditions.

Studies have investigated the roles of TRMs and MDMs under tumor conditions[13,15,21]. TRMs have tumor-promoting roles in driving the responses of regulatory T cell responses, contributing to fibrosis and supporting tumor cell growth[13,15,21]. In pancreatic ductal adenocarcinoma (PDAC), macrophages have divergent roles based on developmental origin, with embryonic-derived TRMs being particularly adept at driving fibrosis[15]. Inflammation and tissue damage during pancreatitis not only is a risk factor for PDAC, but also involves notable accumulation of desmoplastic stroma rich in myeloid cells[22,23]. Macrophages contribute to inflammation during pancreatitis, but the specific contribution of TRMs or MDMs has not been well characterized[24,25]. While the unique ability of the pancreas to respond to injury with substantial desmoplastic stroma is likely critical for preserving function, it is a feature that drives PDAC progression[26,27].

Here, we showed that pancreas TRMs and MDMs increased markedly during pancreatitis and displayed distinct transcriptional phenotypes. We identified a subset of LYVE1^{hi} TRMs that expressed genes related to ECM remodeling, and depletion of TRMs negatively impacted mouse survival during severe acute pancreatitis by attenuating the fibrotic response. TRMs triggered the accumulation of fibroblasts, affected their activation and stimulated the production of collagen and ECM proteins. While TRM-driven fibrosis was protective in pancreatitis, it was co-opted by tumors to support their growth.

Results

Pancreatitis and pancreatic ductal adenocarcinoma display immune cell-rich fibrotic stroma

Pancreatitis and PDAC are characterized by desmoplastic fibrotic stromal responses and immune infiltration[23,28,29]. Histological analysis of human pancreatitis and PDAC tissues both showed marked loss of acinar cell area and increased fibrotic stroma compared to normal tissues (Fig. 1a). Furthermore, we observed increased numbers of CD163$^+$ macrophages, podoplanin$^+$ fibroblasts and trichome$^+$ collagen area in pancreatitis and PDAC tissues compared to normal pancreas (Fig. 1a,b). This indicated shared stromal alterations across the diseased states. To study this in detail, we used serial injection of cerulein in mice, which causes overproduction of digestive enzymes leading to pancreatitis[30]. Compared to vehicle-treated mice, cerulein-treated mice showed widespread acinar-to-ductal metaplasia (ADM) by both histology and immunohistochemistry (IHC) staining for CK19$^+$, Sox9$^+$ and Ki67$^+$ epithelial cells (Fig. 1c,d and Extended Data Fig. 1a). Consistent with widespread inflammation during pancreatitis, we observed increased F4/80$^+$MHCII$^+$ macrophages, F4/80^{lo}MHCII^{lo} eosinophils, Ly6G$^+$ granulocytes and Ly6C$^+$ monocytes in cerulein-treated mice (Fig. 1c,d and Extended Data Fig. 1b,c). Together, these observations highlight the accumulation of macrophages and fibrotic stroma during pancreatitis and PDAC.

### Cerulein treatment increases tissue-resident macrophages

To investigate whether the increase in the number of macrophages in pancreatitis was due to monocyte recruitment or the local expansion of TRMs, we crossed Flt3-Cre mice with R26-LSL-eYFP mice to generate Flt3-YFP mice. In this model, adult bone marrow-derived cells are YFP$^+$, while embryonic-derived macrophages lack YFP expression[31]. While both the numbers of Flt3-YFP$^+$ and Flt3-YFP$^-$ macrophages were increased in cerulein-treated mice compared to vehicle, the number of Flt3-YFP$^-$ macrophages was increased 13-fold, while Flt3-YFP$^+$ macrophages increased 5-fold (Fig. 2a,c and Extended Data Fig. 2a). The frequency of Ki67$^+$ Flt3-YFP$^-$ macrophages was also higher compared to Flt3-YFP$^+$ in cerulein-treated mice (Fig. 2d), indicating TRMs proliferated in situ. To confirm these findings, we next treated CSF1R-mer-iCre-mer;LSL-tdTomato mice (hereafter, CSF1R-tdTom) with a single dose of tamoxifen on embryonic day 9.5 to specifically label embryonic erythro-myeloid progenitor cells. As expected, brain microglia, which are derived from yolk sac[1], showed nearly 80% recombination in CSF1R-tdTom offspring (Fig. 2e–g), while Ly6C^{hi} monocytes showed minimal tdTomato labeling (Fig. 2f). Nearly 10% of pancreas F4/80$^+$MHCII$^{hi/lo}$ macrophages were tdTomato$^+$ (Fig. 2f), indicating a subpopulation of pancreas TRMs was derived from embryonic progenitors. Quantification of tdTomato$^+$ macrophages by flow cytometry and IHC staining indicated that this population expanded during pancreatitis (Fig. 2h–i).

Some embryonically derived macrophages, such as heart or alveolar macrophages, are replaced by MDMs to varying degrees in a tissue-specific manner[6,8,9]. To measure the total TRMs irrespective of developmental origin, we administered tamoxifen by oral gavage in adult CSF1R-tdTom mice for 5 consecutive days, then stopped tamoxifen for 10 weeks to allow monocytes and short-lived MDMs to be washed out, while long-lived TRMs remain tdTomato$^+$ (hereafter we refer to this regimen as pulse-chase; Extended Data Fig. 2b,c). The number of tdTomato$^+$F4/80$^+$MHCII$^+$ TRMs in the pancreas was increased fourfold in cerulein-treated mice compared to vehicle-treated mice (Fig. 2j–m). While CX3CR1-CreERT2 LSL-tdTomato mice (hereafter CX3CR1-tdTom) showed a similar increase in pancreas tdTomato$^+$ TRMs in tamoxifen pulse-chase experiments, a maximum of 50% of pancreas macrophages were tdTomato$^+$ (Extended Data Fig. 2d–k), as reported elsewhere[10]. IHC staining of CX3CR1-tdTom mice indicated that most F4/80$^+$ macrophages in the islets of Langerhans were tdTomato$^+$ TRMs (Extended Data Fig. 2l). Islet macrophages were also tdTomato$^+$ in CSF1R-tdTom tamoxifen pulse-chase mice (Extended Data Fig. 2m). These data suggest that pancreas TRMs consisted of both embryonic-derived and adult HSC-derived cells that expanded numerically during pancreas tissue damage.
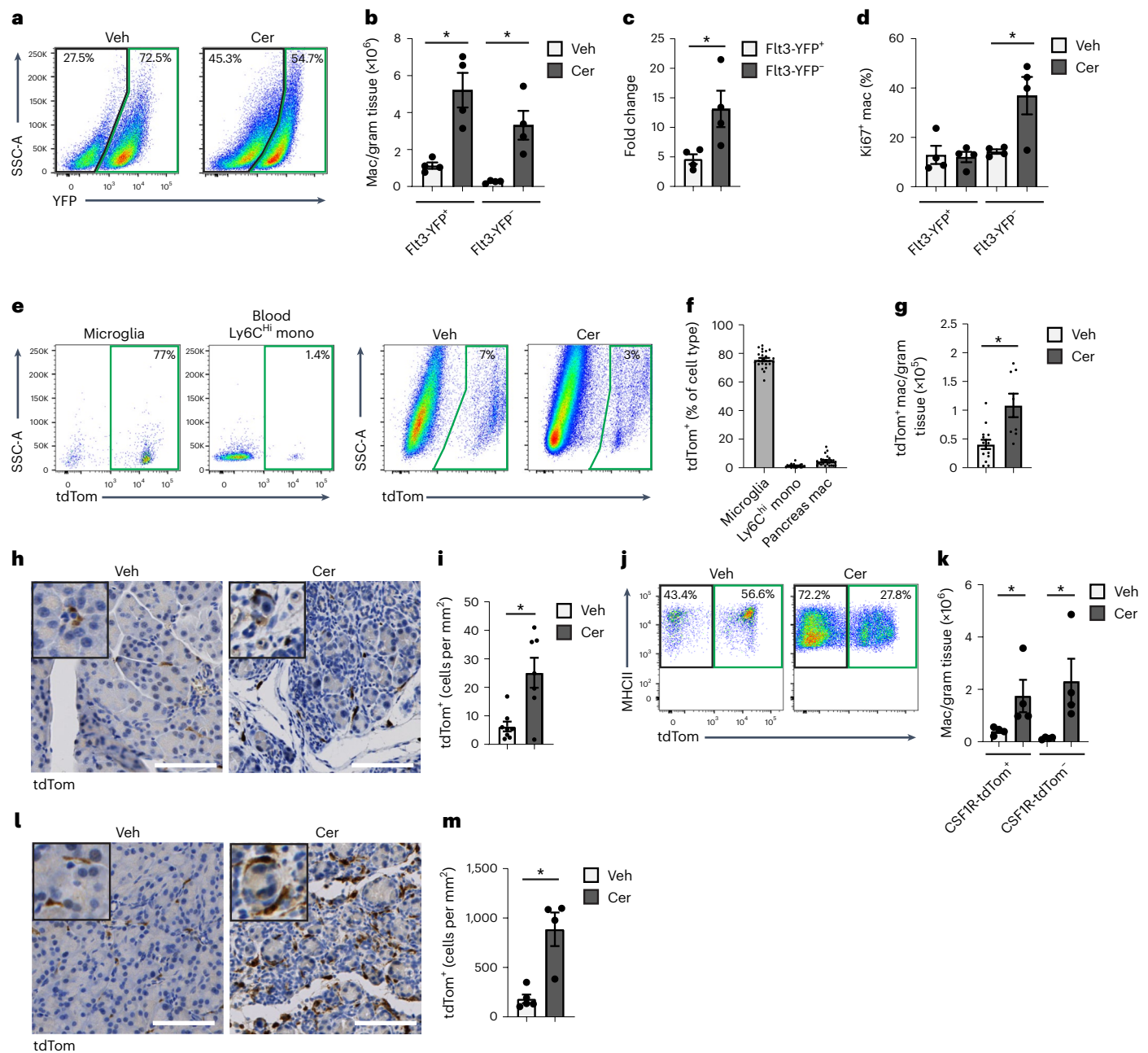
Pancreas tissue-resident macrophages have distinct transcriptional phenotypes

Both ontogeny and tissue of residence can influence TRM phenotype[13,15,18,21,32]. To investigate the ontogeny-dependent roles of macrophages during pancreas injury and cancer, we performed bulk RNA-sequencing (RNA-seq) analysis of pancreas F4/80$^+$MHCII$^+$ macrophages sorted from Flt3-YFP mice treated with vehicle or acute cerulein to induce pancreatitis or implanted orthotopically with PDAC tumors. Differential gene expression analysis identified several thousand differentially expressed genes (DEGs) between Flt3-YFP$^+$ and Flt3-YFP$^-$ macrophages in pancreatitis and PDAC, but only several hundred in the vehicle-treated pancreas (Extended Data Fig. 3a–c). Flt3-YFP$^-$ macrophages highly expressed TRM and alternative-activation genes (for example, Folr2, Cd163, Cd209 and Mrc1), as well as genes related to ECM remodeling (Mmp9, Cert1 and Colec12; Extended Data Fig. 3a). While Flt3-YFP$^-$ macrophages expressed genes linked to collagen production (Col3a1 and Col1a2; Extended Data Fig. 3a), this could be derived from contaminating fibroblasts or mesenchymal cells. Conversely, Flt3-YFP$^+$ macrophages had high expression of antigen-presentation genes, such as H2-Ab1, H2-Eb1 and Cd72 (Extended Data Fig. 3a). Gene-set enrichment analysis (GSEA) indicated that genes upregulated in Flt3-YFP$^-$ macrophages were primarily enriched for pathways related to ECM remodeling and growth factor signaling,
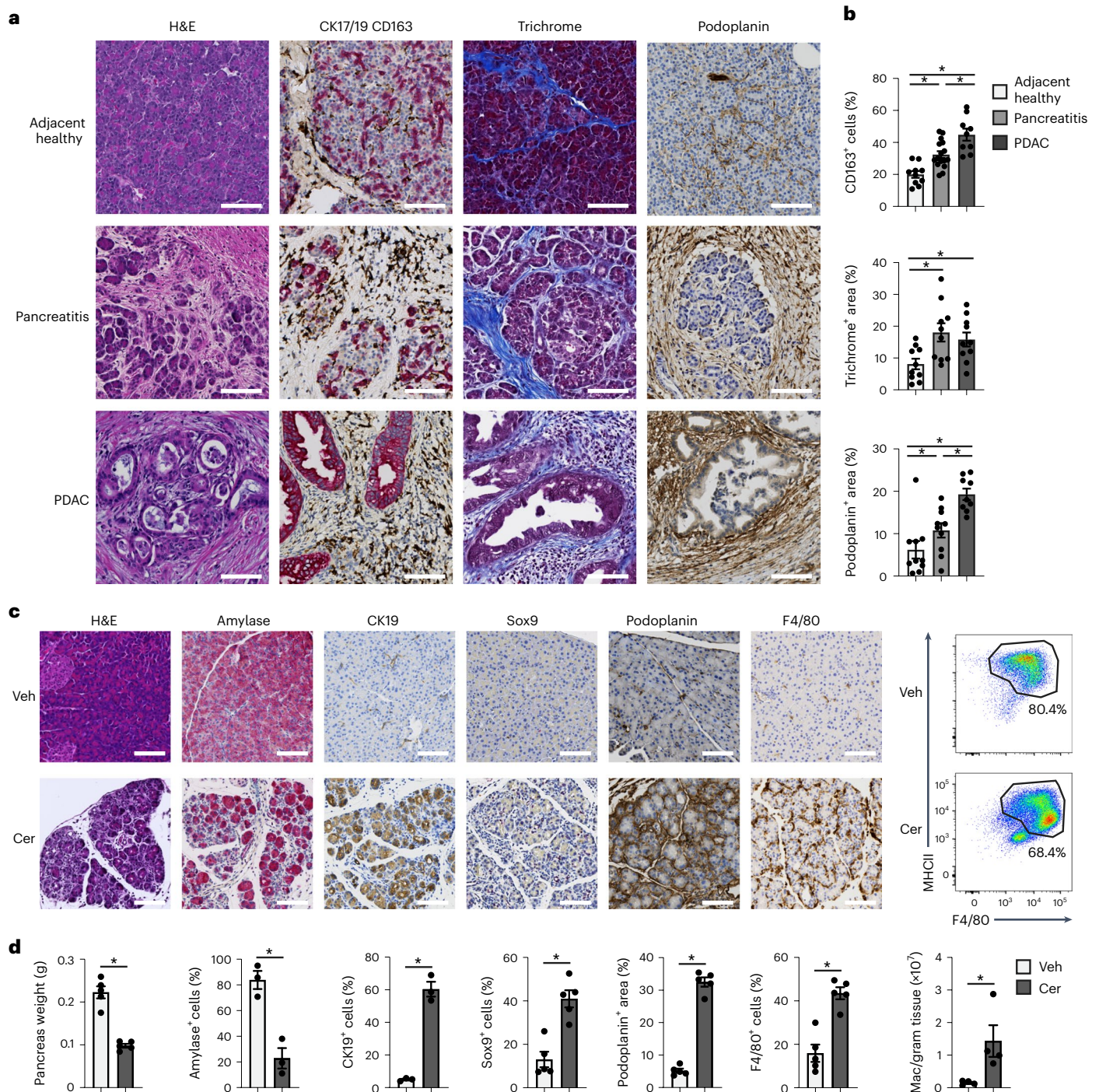
Fig. 1 | Pancreatitis and pancreatic ductal adenocarcinoma display immune rich fibrotic stroma. a, Representative IHC images of hematoxylin and eosin (H&E), CK17/CK19, CD163, trichrome and podoplanin stains on human adjacent healthy pancreas, pancreatitis and PDAC tissue. Scale bars, 100 μm. **b**, Quantification of CD163, trichrome collagen or podoplanin staining in human adjacent healthy pancreas, pancreatitis and PDAC represented as the percentage of cells or the percentage of tissue area. Adjacent healthy, $n = 10$; pancreatitis, $n = 10$; PDAC, $n = 9$. CD163 quantification top to bottom and left to right *$P < 0.0001$, *$P = 0.0039$ and *$P = 0.0051$, trichrome quantification top to bottom and left to right *$P = 0.0232$ and *$P = 0.0115$, and podoplanin quantification top to bottom and left to right *$P = 0.0010$, *$P = 0.0433$ and *$P = 0.0015$) **c**, Representative IHC images of H&E, amylase, CK19, Sox9, podoplanin and

F4/80 and flow cytometry of F4/80$^+$MHCII$^{hi/lo}$ macrophages in the pancreatic tissue from mice treated with vehicle (Veh) or cerulein (Cer) by six hourly i.p. injections every other day for 1 week. Scale bars, 100 μm. **d**, Quantification of pancreas weight, IHC staining with amylase, CK19, Sox9, podoplanin and F4/80 and flow cytometry analysis of F4/80$^+$MHCII$^{hi/lo}$ macrophages in the mouse pancreas as in **c**; (pancreas weight, $n = 5$ mice per group and *$P = 0.0079$; amylase, $n = 3$ mice per group and *$P = 0.0046$; CK19, $n = 3$ mice per group and *$P = 0.0003$; Sox9, $n = 5$ mice per group and *$P = 0.0079$; podoplanin, $n = 5$ mice per group and *$P = 0.0079$; F4/80, $n = 5$ mice per group and *$P = 0.0079$; F4/80$^+$MHCII$^{hi/lo}$ macrophages, $n = 4$ mice per group and *$P = 0.0286$. Data are presented as the mean ± s.e.m. *$P < 0.05$. For comparisons between two groups, Student's two-tailed t-test was used.

Fig. 2 | Cerulein treatment increases tissue-resident macrophages. a, Flow cytometry staining of Flt3-YFP$^+$ and Flt3-YFP$^-$ cells pre-gated on pancreas F4/80$^+$MHCII$^{hi/lo}$ macrophages in Flt3-Cre LSL-YFP (Flt3-YFP) mice. **b**, Density of Flt3-YFP$^+$ and Flt3-YFP$^-$ macrophages in the pancreas of Flt3-YFP mice after six hourly i.p. injections with Veh or Cer every other day for 1 week; n = 4 mice per group, left to right *P = 0.0052 and *P = 0.0077. **c**, Fold change in the density of Flt3-YFP$^+$ and Flt3-YFP$^-$ macrophages in Flt3-YFP mice treated with Veh or Cer as in **b**; n = 4 mice per group, *P = 0.0286. **d**, Percentage of Flt3-YFP$^+$ and Flt3-YFP$^-$ macrophages that expressed Ki67 in Veh-treated or Cer-treated Flt3-YFP mice as in **b**; n = 4 mice per group, *P = 0.0251. **e**, Flow cytometry of brain CD45$^+$F4/80^{lo} microglia, blood Ly6C^{hi} monocytes and pancreas F4/80$^+$MHCII$^{hi/lo}$ macrophages in CSF1R-tdTom mice treated in utero with tamoxifen on embryonic day 9.5 (9 d after vaginal plug appearance) followed by treatment with Veh or Cer starting at 8 weeks of age as in **b**. **f**, Percentage of brain CD45$^+$F4/80^{lo} microglia, blood Ly6C^{hi} monocytes and pancreas F4/80$^+$MHCII$^{hi/lo}$ macrophages labeled by tdTomato in CSF1R-tdTom mice treated with tamoxifen followed by Veh or Cer as in **e**; n = 24 mice/cell type analyzed. **g**, Density of pancreas F4/80$^+$MHCII$^{hi/lo}$

macrophages labeled by tdTomato in CSF1R-tdTom mice treated with tamoxifen followed by Veh or Cer as in **e**; Veh, n = 14 mice; Cer, n = 8 mice, *P = 0.0022. **h**, Representative images of IHC stain for tdTomato in pancreas tissue from CSF1R-tdTom mice treated with tamoxifen followed by Veh or Cer as in **e**. **i**, Quantification of tdTomato$^+$ cells in pancreas tissue of CSF1R-tdTom mice treated with tamoxifen followed by Veh or Cer as in **e**; Veh, n = 8 mice; Cer, n = 7 mice, *P = 0.0289. **j**, Flow cytometry of tdTomato expression in pancreas F4/80$^+$MHCII$^{hi/lo}$ macrophages in CSF1R-tdTom mice administered tamoxifen by oral gavage for five consecutive days, followed by 10 weeks rest and then treated with Veh or Cer as in **b**; n = 4 mice per group. **k**, Density of pancreas tdTomato$^+$ and tdTomato$^-$ macrophages in CSF1R-tdTom mice as in **j**; n = 4 mice per group, left to right *P = 0.0286 and *P = 0.0286. **l**, Representative images of IHC stain for tdTomato on pancreas from CSF1R-tdTom as in **j**; n = 4 mice per group. **m**, Quantification of pancreas tdTomato$^+$ macrophages from CSF1R-tdTom mice as in **j**; n = 4 mice per group, *P = 0.0159. Data are presented as the mean ± s.e.m. *P < 0.05. For comparisons between two groups, Student's two-tailed t-test was used.

while Flt3-YFP⁺ macrophages were enriched for antigen-presentation and T cell activation pathways (Extended Data Fig. 3b). Some of these differences were specific to tissue damage, rather than homeostasis (Extended Data Fig. 3c).

To determine whether embryonically derived and HSC-derived TRMs defined phenotypically unique or mixed populations, we performed single-cell RNA sequencing (scRNA-seq). We sorted Flt3-YFP⁺ and Flt3-YFP⁻ F4/80⁺MHCII⁺ macrophages from vehicle-treated (healthy pancreas), cerulein-treated (pancreatitis) and PDAC tumors. We also analyzed tumor-bearing liver and lung, as a positive control for an embryonic TRM population (liver Kupffer cells) and mixed TRM-MDM (alveolar macrophages)[4,6,7,9]. As expected, liver and lung macrophages showed origin-specific clustering in scRNA-seq analysis (Fig. 3a,b and Extended Data Fig. 3d–f). By contrast, in the pancreas, most macrophage scRNA-seq clusters were of mixed origin, with contribution from Flt3-YFP⁺ and Flt3-YFP⁻ macrophages (Fig. 3c,d). The only exception was *Lyve1*ʰⁱ clusters (vehicle cluster 0, cerulein cluster 2 and PDAC cluster 5; Fig. 3e and Extended Data Fig. 4a–d), which showed up to 90% enrichment for Flt3-YFP⁻ macrophages (Fig. 3c–e and Extended Data Fig. 4a–h). Some *Lyve1*ˡᵒ clusters (vehicle clusters 2 and 4, and cerulein cluster 4) showed a bias toward Flt3-YFP⁺ cells and were marked by high expression of *Ccr2* and MHCII family genes (Fig. 3c–e). Other mixed-origin *Lyve1*ˡᵒ clusters expressed *Trem2* and *Cx3cr1* (Extended Data Fig. 4e–h). This suggests that, aside from *Lyve1*ʰⁱ TRMs, most TRMs are of mixed origin, and their transcriptional phenotypes might be defined by tissue cues.

Because most pancreas clusters were of mixed origin, we investigated the impact of origin on macrophage phenotype. Pseudobulk analysis of the scRNA-seq data, irrespective of clusters, showed enrichment in ECM and ECM remodeling signatures and antigen processing and presentation in Flt3-YFP⁻ and Flt3-YFP⁺ macrophages, respectively (Fig. 3f). Of note, the Flt3-YFP⁻ macrophages in the scRNA-seq clusters did not show expression of collagen genes, indicating that expression of collagen in the bulk RNA-seq might have been due to contamination with other cell types. Next, we assessed how origin might impact phenotype within a single cluster. Comparison of Flt3-YFP⁻ and Flt3-YFP⁺ cells in pancreatitis cluster 0 indicated that Flt3-YFP⁻ cells were enriched for TNF signaling by NF-κB, inflammatory responses and TGF-β signaling, while Flt3-YFP⁺ cells showed higher expression of oxidative phosphorylation and Myc targets (Extended Data Fig. 4g). These data suggest that even in mixed-origin macrophage subsets, origin may yield subtle phenotypic differences.

We next investigated whether *Lyve1*ʰⁱ macrophages consisted predominantly of long-lived TRMs. scRNA-seq on F4/80⁺MHCII⁺ macrophages sorted from pancreas tissue of CSF1R-tdTom mice pulse-chased with tamoxifen showed that clusters of *Lyve1*ʰⁱ macrophages were predominantly tdTomato⁺, while *Lyve1*ˡᵒ clusters showed mixed labeling (Fig. 3g–i), suggesting pancreas *Lyve1*ʰⁱ macrophages were predominantly embryonically derived, long-lived TRMs. As before, *Lyve1*ʰⁱ macrophage clusters expressed scavenger receptors and alternative-activation markers (*Cd163*, *Siglec1*, *Timd4*, *Cd209* and *Mrc1*) and showed enrichment in ECM and ECM remodeling genes and gene sets (Fig. 3j–m and Extended Data Fig. 5a,b). *Lyve1*ˡᵒ macrophage clusters highly expressed *H2-Aa*, *H2-Ab1*, *H2-Eb1*, *Cd52* and *Cd72* and showed enrichment in T cell activation, major histocompatibility complex (MHC) and NF-κB signaling pathways (Fig. 3j–m). Pseudobulk analysis comparing all tdTomato⁺ and tdTomato⁻ cells, irrespective of cluster, identified similar gene sets (Extended Data Fig. 5a,b). This analysis suggested that *Lyve1*ʰⁱ macrophages were embryonic TRMs with a unique transcriptional phenotype.

To determine possible localization differences in LYVE1⁺ TRMs, we performed multiplex immunohistochemistry (mIHC). Pancreas tissue from CSF1R-tdTom tamoxifen pulse-chase mice treated with cerulein for 1 week was stained for F4/80, LYVE1, tdTomato and CK19, and showed more than 80% of F4/80⁺LYVE1ʰⁱ cells were tdTomato⁺ and were located between the lobules of the pancreas and rarely in close contact with acinar cells or within islets (Fig. 3n and Extended Data Fig. 5c). This distribution was not observed for other tdTomato⁺ TRMs, some of which showed infiltration between clusters of acinar cells (Fig. 3n), suggesting that LYVE1ʰⁱ TRMs had distinct regional distributions within the pancreas. Finally, to test the tissue residence of the LYVE1⁺ macrophages, we treated healthy, surgically joined CD45.1 and CD45.2 mice with vehicle or cerulein for 1 week at week 6 after surgery. At week 1 of cerulein or vehicle treatment, Ly6C⁺ blood monocytes were 20–30% of parabiotic donor origin, while LYVE1⁺CD163⁺ pancreas macrophages were 4% of donor origin (Extended Data Fig. 5d–f). Around 15–20% of LYVE1⁻CD163⁻ and MHCII⁺ pancreas macrophages were of donor origin (Extended Data Fig. 5d–f), suggesting they were MDMs. While most recruited monocytes had an LYVE1⁻CD163⁻ or MHCIIʰⁱ MDM profile, 11% were CD163⁺, indicating a TRM phenotype (Extended Data Fig. 5f). In total, these data suggest that LYVE1⁺ macrophage phenotypes and localization might contribute to pathologic fibrosis during pancreas injury.
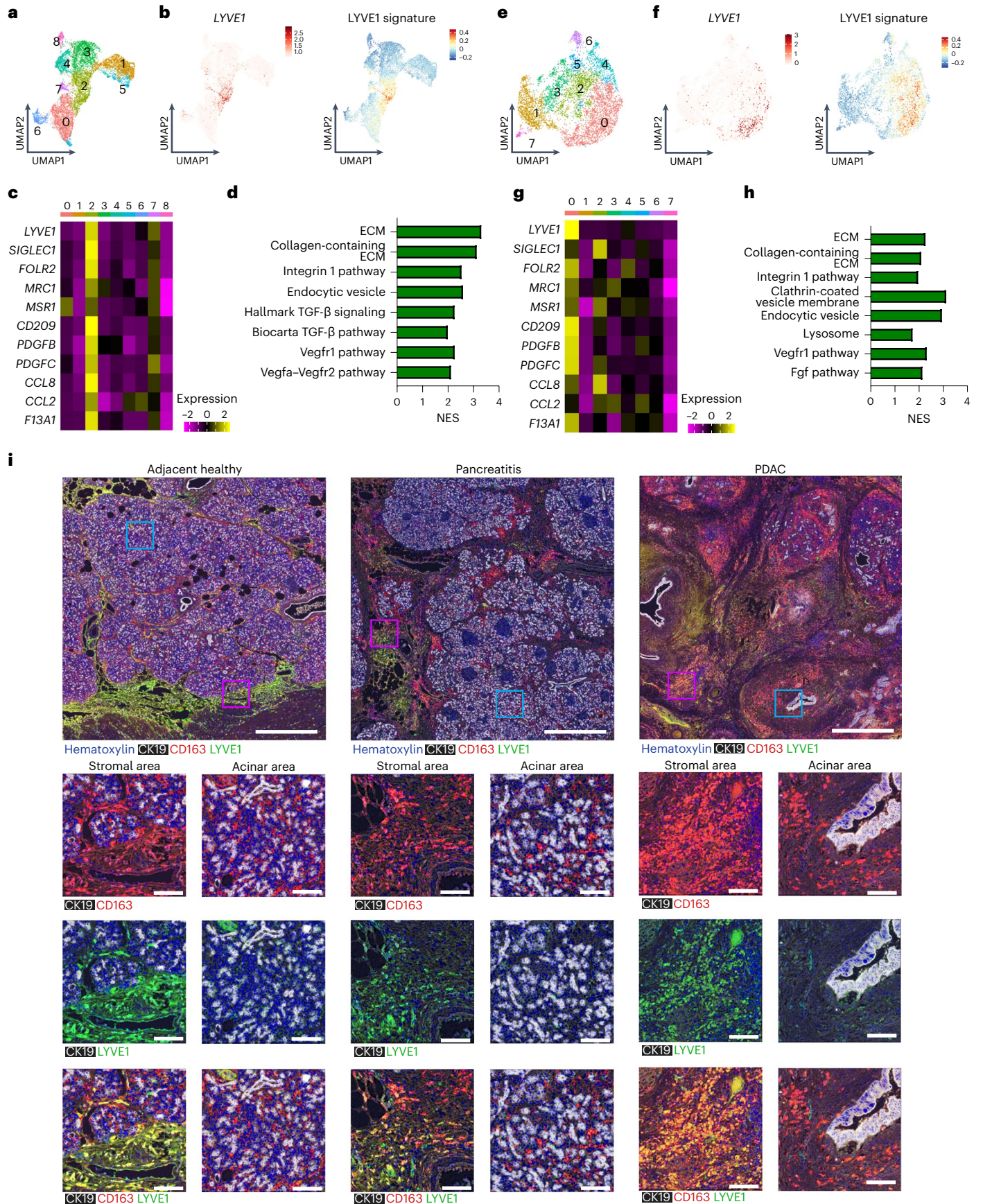
Human LYVE1⁺ tissue-resident macrophages display similar phenotype and localization

To compare macrophage subsets in human pancreas tissues[33,34], we identified clusters of macrophages and monocytes in publicly available scRNA-seq data from three healthy and nine chronic pancreatitis tissues[34]. We first mapped the gene expression signature of mouse *Lyve1*ʰⁱ macrophages using an averaged z-score. This signature was most highly expressed in human cluster 2, which was the only human cluster with

Fig. 3 | Pancreas tissue-resident macrophages have distinct transcriptional phenotypes. a, UMAP plot from scRNA-seq analysis of F4/80⁺MHCIIʰⁱ/ˡᵒ macrophages sorted from livers of Flt3-YFP mice on day 14 after implantation with the KP2 pancreatic cancer cell line. **b**, Quantification of Flt3-YFP⁺ and Flt3-YFP⁻ macrophages by cluster from UMAP in **a**, displayed as the percentage of each cluster. **c**, UMAP plot of scRNA-seq analysis of F4/80⁺MHCIIʰⁱ/ˡᵒ macrophages sorted from the pancreas of Flt3-YFP mice treated with six hourly i.p. injections of Cer every other day for 1 week. **d**, Quantification of Flt3-YFP⁺ and Flt3-YFP⁻ macrophages by cluster from UMAP in **c**, displayed as the percentage of each cluster. **e**, UMAP plots displaying *Lyve1*, *Cx3cr1*, *Ccr2*, *H2-Ab1*, *Cd163* and *Mrc1* gene expression in *Csf1r*- and *C1qa*-expressing pancreas macrophages from Flt3-YFP mice as in **c**. **f**, Heat map displaying normalized enrichment score (NES) of significantly enriched gene sets comparing all Flt3-YFP⁻ macrophages versus Flt3-YFP⁺ macrophages in indicated single-cell datasets; pathways selected by false discovery rate (FDR) < 0.05. **g**, UMAP plot of scRNA-seq analysis of F4/80⁺MHCIIʰⁱ/ˡᵒ macrophages sorted from the pancreas of CSF1R-tdTom mice administered tamoxifen by oral gavage for 5 consecutive days, followed by a rest period of 10 weeks and a regimen of six hourly Cer i.p. injections every other day for 1 week. **h**, Quantification of tdTom⁻ and tdTom⁺ macrophages by cluster from UMAP in **g**, displayed as the percentage of each cluster. **i**, UMAP plots of *Lyve1*, *Cx3cr1*, *Ccr2* and *H2-Ab1* expression in *Csf1r*- and *C1qa*-expressing pancreas macrophages from CSF1R-tdTom mice as in **g**. **j**, Heat map of DEGs upregulated in either LYVE1ʰⁱ or LYVE1ˡᵒ macrophages across healthy pancreas, pancreatitis and PDAC samples from Flt3-YFP mice treated with vehicle (healthy) or cerulein (pancreatitis) as in **c**, or orthotopically implanted with the KP1 pancreatic cancer cell line (PDAC). **k**, Bar graph of NES values of gene sets in LYVE1ʰⁱ and LYVE1ˡᵒ macrophages as in **j**. **l**, Heat map of DEGs upregulated in either LYVE1ʰⁱ or LYVE1ˡᵒ macrophages from the pancreas of CSF1R-tdTom mice treated as in **g**. **m**, Bar graph of NES values of gene sets in LYVE1ʰⁱ to LYVE1ˡᵒ macrophages as in **l**. **n**, Representative images from mIHC staining for hematoxylin, F4/80, tdTomato, LYVE1 and CK19 in the pancreas of cerulein-treated CSF1R-tdTom mice treated as in **g**, with staining repeated for four Veh-treated and four Cer-treated mice. Data are presented as the mean ± s.e.m. unless otherwise indicated. *P < 0.05. For comparisons between two groups, Student's two-tailed t-test was used, except for **j** and **l**, where Bonferroni correction was used, and **f**, **k** and **m**, where FDR was used.
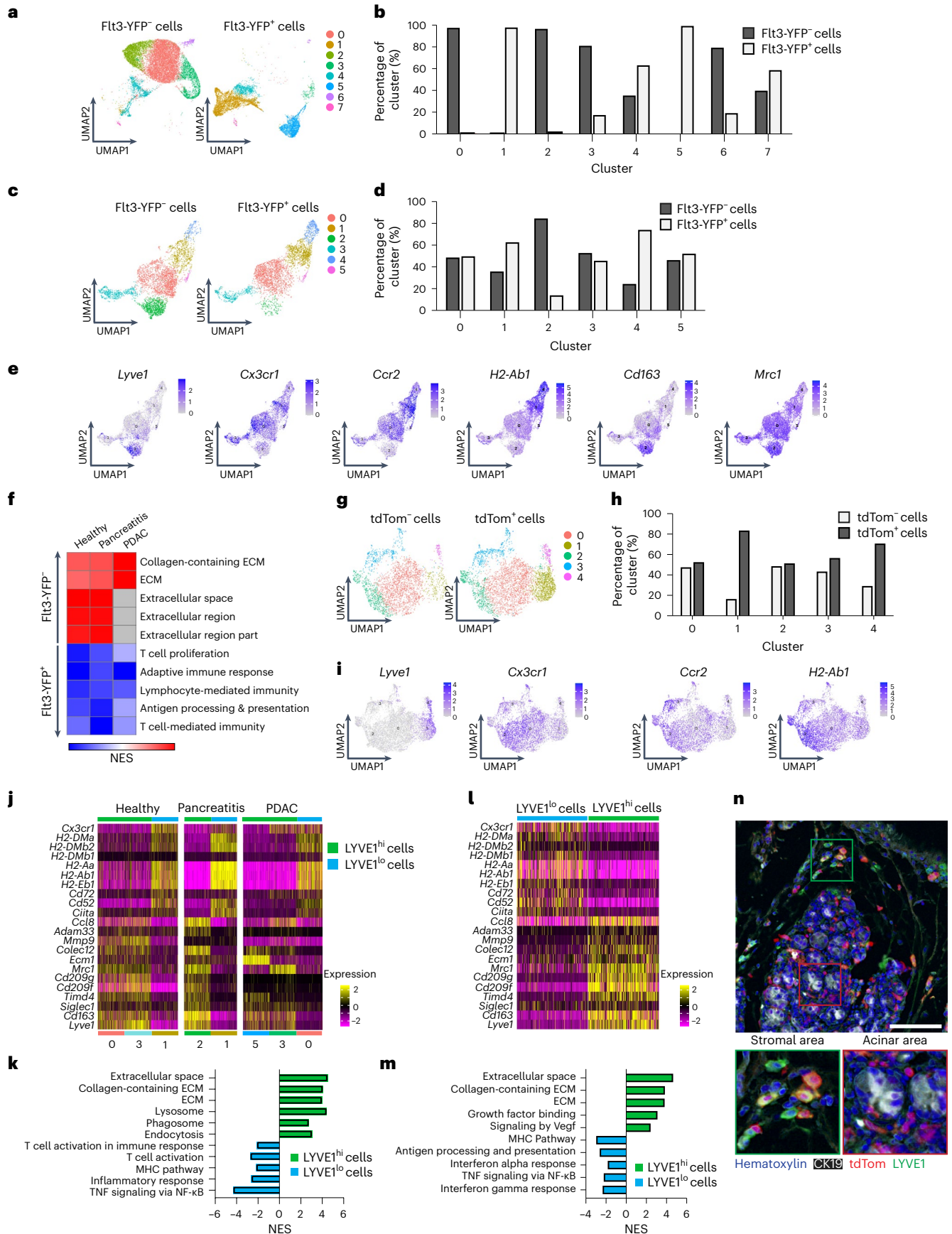
Fig. 4 | Human LYVE1⁺ tissue-resident macrophages display similar phenotype and localization. a, UMAP of scRNA-seq analysis in monocytes/macrophages from a published human chronic pancreatitis dataset[34], including three healthy pancreas, four idiopathic and five hereditary chronic pancreatitis samples. **b**, UMAP plots showing *LYVE1* gene expression and mouse LYVE1^{hi} macrophage scRNA-seq signatures using the top 100 DEGs from mouse LYVE1^{hi} macrophages mapped into healthy and chronic pancreatitis samples from **a**. **c**, Heat map of select marker genes differentially expressed in human chronic pancreatitis cluster 2. Data are significant at $P < 0.05$ using Bonferroni correction. **d**, Bar graph of NES values of gene sets enriched in LYVE1^{hi} macrophages from human chronic pancreatitis (cluster 2) compared to all other clusters. Data are FDR < 0.05 significant. **e**, UMAP of scRNA-seq analysis in monocytes/macrophages from 16 human PDAC samples from a published PDAC dataset[33].

f, UMAP plots of *LYVE1* gene expression and mouse LYVE1^{hi} macrophage scRNA-seq signature using the top 100 DEGs from mouse LYVE1^{hi} macrophages mapped into PDAC samples from **f**. **g**, Heat map of select marker genes differentially expressed in the human PDAC cluster 0. Data are significant at $P < 0.05$ using Bonferroni correction. **h**, Bar graph of NES values of gene sets enriched in human PDAC LYVE1^{hi} macrophages (cluster 0) compared to all other clusters. Data are FDR < 0.05 significant. **i**, Representative mIHC images from adjacent healthy pancreas or pancreatitis and PDAC tumor samples obtained from individuals at Barnes-Jewish Hospital stained for hematoxylin, CK19, CD163 and LYVE1. Highlighted areas of stromal or acinar area showing CK19 and CD163, CK19 and Lyve1, or CK19, CD163 and LYVE1 merged. Scale bars, 1 mm (top row) or 100 μM (bottom three rows).

significant expression of the *LYVE1* gene (Fig. 4a,b). Human cluster 2 expressed similar marker genes to mouse *Lyve1*^{hi} macrophages, including *FOLR2*, *MRC1* and *PDGFC* (Fig. 4c). By GSEA analysis, human *LYVE1*^{hi} macrophages (cluster 2) had enrichment in ECM remodeling, TGF-β signaling and VEGF pathways (Fig. 4d). In publicly available human PDAC scRNA-seq datasets[33], cluster 0 was enriched for the mouse *Lyve1*^{hi} signature, had *LYVE1* gene expression, and had similar phenotypes to both mouse and human pancreatitis *Lyve1*^{hi} clusters by GSEA (Fig. 4e,h). The mouse *Lyve1*^{lo} macrophage signature was found in most other human macrophage clusters (Extended Data Fig. 6a,b). mIHC for CD163, LYVE1 and CK19 on human healthy pancreas, pancreatitis and PDAC tissues showed that CD163 expression was more ubiquitous across macrophage subsets in humans than in mice (Fig. 4i). However, expression of LYVE1 was limited to a subset of CSF1R⁺CD68⁺CD163⁺ cells (Extended Data Fig. 6c–f). In human pancreatitis and PDAC tissues, LYVE1⁺CD163⁺ macrophages were only detected within the stroma and outside of acinar areas, while LYVE1⁻CD163⁺ macrophages were localized in both compartments (Fig. 4i). These data suggest conservation in phenotype and localization between mouse and human LYVE1⁺ pancreas macrophages.

Tissue-resident macrophages maintain tissue integrity during pancreatitis

We next asked whether TRMs and MDMs have a distinct functional impact during pancreatitis. To deplete TRMs, mice were treated with either the combination of CSF1 neutralizing antibodies and clodronate-loaded liposomes (CSF1Ab-CLD)[15,35] or control antibodies and PBS-loaded liposomes (IgG-PBS). Mice were then rested for 10 d to allow the recovery of blood Ly6C^{hi} monocytes and MDMs, and then

treated with cerulein or vehicle by intraperitoneal (i.p.) injection for 7 d. At day 10 after CSF1Ab-CLD treatment, before the cerulein treatment, blood Ly6C^{lo} monocytes were reduced compared to IgG-PBS control mice (Fig. 5a,b), while the total number of pancreas F4/80⁺MHCII⁺ macrophages was notably reduced (Fig. 5b and Extended Data Fig. 7a–c). At day 7 of cerulein treatment, CSF1Ab-CLD mice still had reduced numbers of pancreas F4/80⁺MHCII⁺ macrophages compared to IgG-PBS controls, despite having normal numbers of circulating Ly6C^{hi} monocytes (Fig. 5b). mIHC indicated that F4/80⁺LYVE1⁺CD163⁺ TRMs were reduced more than 90% in CSF1Ab-CLD + cerulein mice (Fig. 5c). To investigate the effect of TRM loss on pathogenesis, CSF1Ab-CLD or IgG-PBS mice were implanted with osmotic pumps that administered cerulein or vehicle for up to 14 d. In IgG-PBS control mice, we observed acute body weight loss at days 2–5 after cerulein, followed by recovery at days 6–9 after cerulein (Fig. 5d). By contrast, CSF1Ab-CLD-treated mice continually lost body weight after cerulein pump implantation and reached humane survival endpoints by week 1 (Fig. 5d,e). Similar observations were made with both 8 μg per day and 10 μg per day dosages of cerulein and FvB and C57BL/6 mice (Fig. 5d,e and Extended Data Fig. 7d,e). Along with impaired survival, CSF1Ab-CLD-treated mice had a significant decrease in blood glucose and an increase in serum amylase during pancreatitis compared to IgG-PBS mice (Extended Data Fig. 7f–i). Histologic analysis of the pancreas tissues indicated loss of pancreas tissue integrity, substantial tissue necrosis and 90% loss of amylase⁺ acinar cells and CK19⁺ ductal cells and an increase in cleaved caspase-3⁺ cells in CSF1Ab-CLD-treated mice compared to IgG-PBS mice (Fig. 5f–h). In contrast, we observed no histologic difference in the livers of CSF1Ab-CLD and IgG-PBS mice (Extended Data Fig. 7i), suggesting a pancreas-specific defect.

**Fig. 5 | Tissue-resident macrophages maintain tissue integrity during pancreatitis. a**, Flow cytometry plots of blood Ly6C^{hi} monocytes and pancreas F4/80⁺MHCII[hi/lo] macrophages from wild-type mice that received CSF1 antibody and CLDs (CSF1Ab + CLD) or IgG and PBS-loaded liposomes (IgG + PBS) by i.p. injection, then allowed to recover for 10 d (day −1), followed by six hourly i.p. injections of Cer every other day for 1 week (day 7). **b**, Quantification of blood Ly6C^{lo} and Ly6C^{hi} monocytes after the recovery period (day −1), and pancreas F4/80⁺MHCII[hi/lo] macrophages after the recovery period (day −1) and after Cer treatment (day 7) in mice treated as in **a**. Blood Ly6C^{lo} and Ly6C^{hi}, $n = 4$ mice per group; pancreas F4/80⁺MHCII[hi/lo] macrophages IgG + PBS day −1, $n = 4$ mice per group, all other, $n = 3$ mice per group, left to right $*P = 0.0012$ and $*P = 0.0002$. **c**, Representative mIHC staining for hematoxylin, F4/80, LYVE1, CD163 and CK19 in the pancreas and quantification of pancreas F4/80⁺LYVE1⁺CD163⁺ macrophages, displayed as the percentage of cells, in mice as in **a**; IgG + PBS, $n = 6$ mice per group, CSF1Ab + CLD, $n = 7$ mice per group, $*P = 0.0006$. Scale bars, 100 μm. **d**, Body weight measurement in mice treated with IgG + PBS or CSF1Ab + CLD and implanted 10 d later in the peritoneal cavity with osmotic pumps for the delivery of dimethylsulfoxide (DMSO; control), 8 μg per day cerulein or 10 μg per day cerulein. Measurements starting on day of osmotic pump implantation; DMSO, $n = 5$ mice, all other, $n = 10$ mice. **e**, Kaplan–Meier survival curve showing mice treated with IgG + PBS and CSF1Ab + CLD followed by osmotic pump

implantation as in **e**; $n = 10$ mice per group. IgG + PBS versus CSF1Ab + CLD with 10 μg per day cerulein, $P = 0.0001$; IgG + PBS versus CSF1Ab + CLD with 8 μg per day cerulein, $P < 0.0001$. **f**, Representative images of pancreas tissue stained for H&E, CK19, amylase or cleaved caspase-3 (CC3) from mice treated with IgG + PBS or CSF1Ab + CLD followed by osmotic pump delivery of 10 μg per day Cer, as in **e**, taken at humane survival endpoint (top two rows) or at day 6 after osmotic pump implantation (bottom row). Scale bars, 100 μm. **g**, Quantification of CK19, amylase and CC3 IHC stains in pancreas tissue from IgG + PBS or CSF1Ab + CLD-treated mice administered 10 μg per day Cer by osmotic pump, as in **e**, at humane survival endpoint, displayed as the percentage of cells; CK19, $n = 5$ mice per group and $*P = 0.0079$; amylase, IgG + PBS, $n = 9$ mice, amylase CSF1Ab + CLD, $n = 8$ mice, $*P < 0.0001$; CC3, $n = 10$ mice per group and $*P < 0.0001$. **h**, Quantification of CK19, amylase and CC3 IHC stains in pancreas tissue from IgG + PBS or CSF1Ab + CLD-treated mice administered 10 μg per day Cer by osmotic pump, as in **e**, at day 6 after osmotic pump implantation, displayed as the percentage of cells; IgG + PBS, $n = 12$ mice; CSF1Ab + CLD, $n = 11$ mice; CK19, $*P < 0.0001$; amylase, $n = 10$ mice per group, $*P = 0.0089$; CC3, $n = 10$ mice per group and $*P < 0.0001$. Data are presented as the mean ± s.e.m. unless otherwise indicated. $*P < 0.05$. For comparisons between two groups, Student's two-tailed t-test was used.

To test the role of MDMs in pancreatitis progression, we used CCR2-deficient mice (CCR2-KO), which have impaired egress of Ly6C^{hi} monocytes from the bone marrow[36] resulting in reduced numbers of blood Ly6C^{hi} monocytes (Extended Data Fig. 7j). We observed normal numbers of total F4/80[+] macrophages in steady-state pancreas tissues compared to wild-type mice (Extended Data Fig. 7j). Cerulein-treated CCR2-KO mice had no change in total pancreas F4/80[+] macrophages

(Extended Data Fig. 7j), but a decrease in the number of pancreas MHCII[hi] macrophages compared to wild-type mice (Extended Data Fig. 7j). CCR2-KO and wild-type mice had similar survival and pancreas weight following cerulein-loaded osmotic pump implantation (Extended Data Fig. 7k). Together, this suggests that TRMs are critical in restoring pancreas tissue homeostasis after acute damage, whereas MDMs are largely dispensable.

Hematoxylin Amylase CK19 Sox9 Ki67 Podoplanin

Hematoxylin CK19 LYVE1 CD163
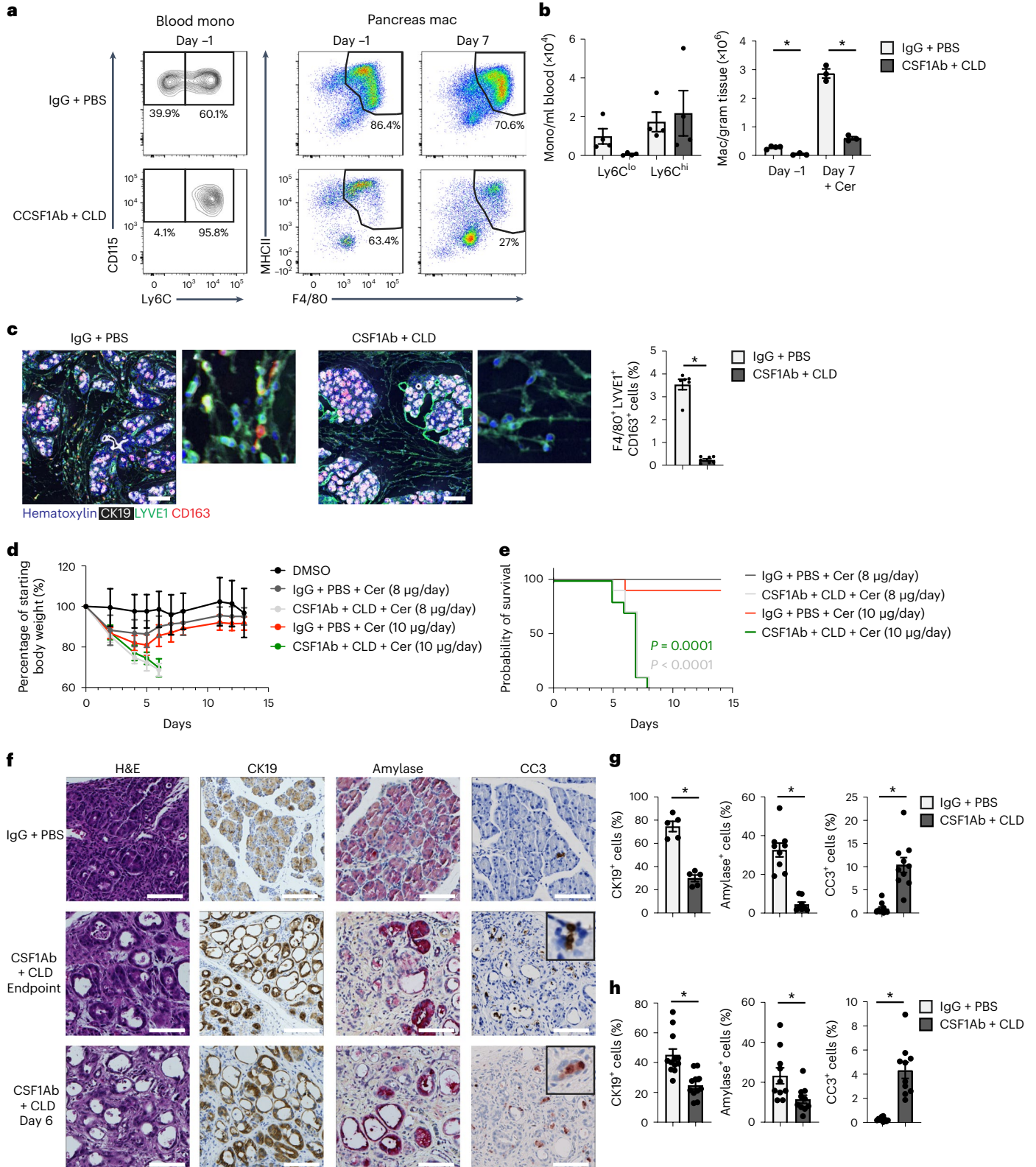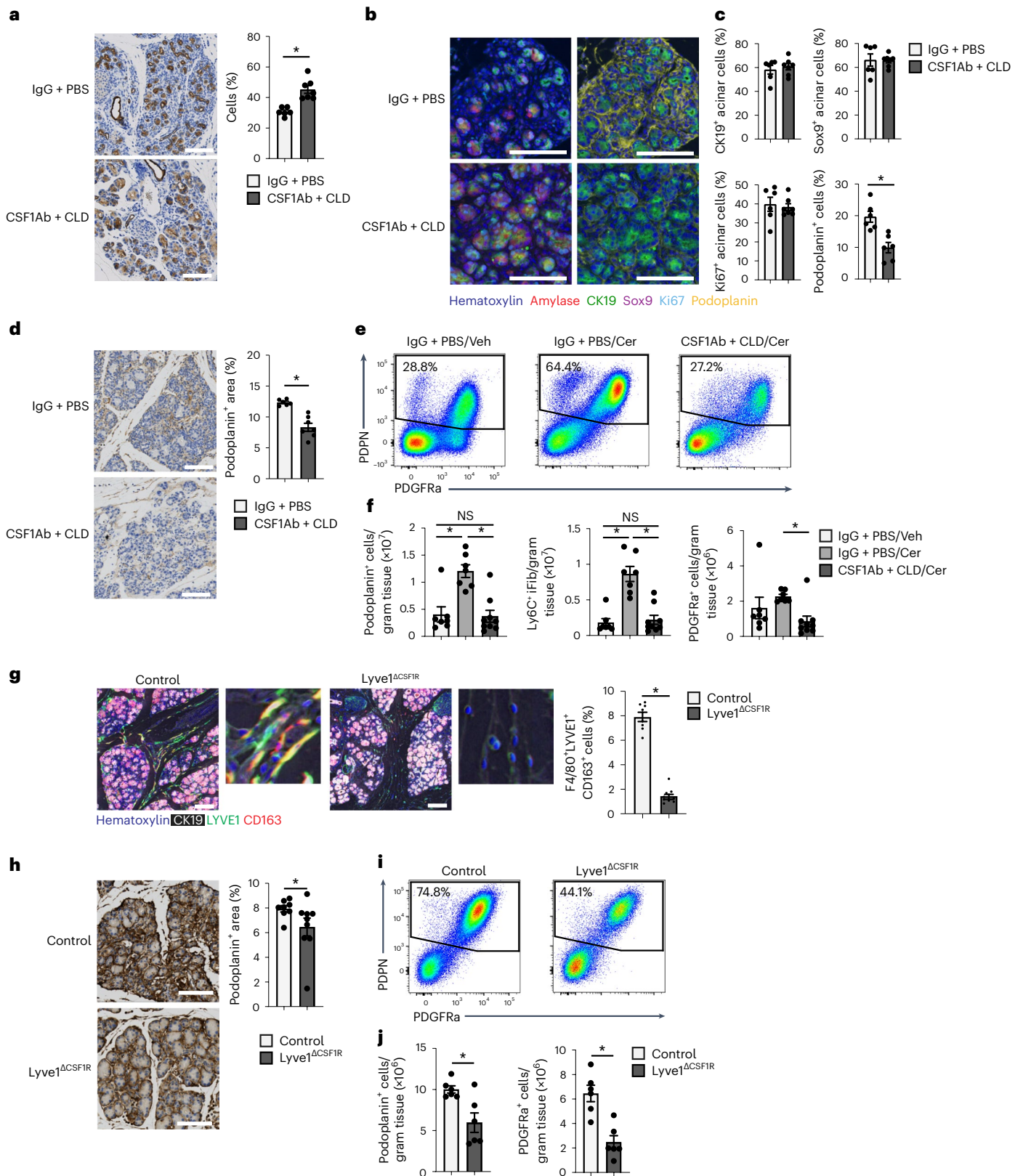
Depletion of tissue-resident macrophages attenuates fibrotic responses

To address whether the protective effect of TRMs was due to changes in the ADM process, we injected mice with CSF1Ab-CLD or IgG-PBS, waited 10 d, then injected cerulein or vehicle by six hourly i.p. injections (that is, once per hour for 6 h) every other day for 1 week. By IHC, CSF1Ab-CLD mice had an increased percentage of CK19+ cells in the

pancreas compared to IgG-PBS controls (Fig. 6a). Close examination indicated CSF1Ab-CLD mice had significantly fewer stromal cells and stromal area between the acinar cell clusters (Fig. 6a). mIHC using the ADM markers CK19, Sox9 and Ki67 showed no difference in the percentage of amylase+ acinar cells expressing CK19, Sox9 or Ki67 between CSF1Ab-CLD and IgG-PBS mice (Fig. 6b,c), indicating that TRM depletion did not affect the ability of acinar cells to undergo ADM. In contrast,

Fig. 6 | Depletion of tissue-resident macrophages attenuates fibrotic responses. a, Representative images and quantification of CK19 IHC stain on pancreas tissue of mice treated with IgG + PBS or CSF1Ab + CLD, followed by a 10-d recovery period, then six hourly i.p. injections with Cer every other day for 1 week; IgG + PBS, n = 6 mice; CSF1Ab + CLD, n = 7 mice and *P = 0.0012. **b**, Representative mIHC images of pancreas tissue from mice treated as in **a**, stained for hematoxylin, amylase, CK19, Sox9, Ki67 and podoplanin, Scale bars, 100 μm. **c**, Quantification of amylase$^+$ acinar cells expressing CK19, Sox9 or Ki67, displayed as the percentage of acinar cells, and podoplanin$^+$ cells, displayed as the percentage of total cells; IgG + PBS, n = 6 mice; CSF1Ab + CLD, n = 7 mice; and *P = 0.0022 for podoplanin analysis. **d**, Representative images of pancreas tissue stained for podoplanin and quantification of podoplanin$^+$ area in pancreas from mice treated as in **a**; IgG + PBS, n = 6 mice; CSF1Ab + CLD, n = 7 mice and *P = 0.0012. **e**, Flow cytometry plots of IgG + PBS $^+$ pancreas fibroblasts from IgG + PBS-treated mice injected i.p. with Veh (IgG + PBS/Veh), or IgG + PBS-treated or CSF1Ab + CLD-treated mice injected i.p. with Cer (IgG + PBS/Cer or CSF1Ab + CLD/Cer), as in **a**. **f**, Density of pancreas IgG + PBS$^+$ fibroblasts, Ly6C$^+$ iFibs and PDGFRa$^+$ fibroblasts from IgG + PBS/Veh, IgG + PBS/Cer or CSF1Ab + CLD/Cer mice as in **e**; IgG + PBS/Veh, n = 7 mice; IgG + PBS/Cer, n = 7

mice; CSF1Ab + CLD/Cer, n = 9 mice; top to bottom and left to right, *P = 0.0005 and *P = 0.0003 in podoplanin analysis, *P < 0.0001 and *P < 0.0001 in Ly6C$^+$ iFib analysis, and *P = 0.0409 in PDGFRa analysis. **g**, Representative mIHC images of pancreas tissue from Lyve1-Cre$^-$ mice (control) or Lyve1-CreCSF1R$^{flox/flox}$ mice (Lyve1^{ΔCSF1R}) treated with six hourly i.p. injections of Cer every other day for 1 week, stained for hematoxylin, CK19, F4/80, LYVE1 and CD163 and quantification of F4/80$^+$LYVE1$^+$CD163$^+$ pancreas macrophages from control or Lyve1^{ΔCSF1R} mice treated with Cer, displayed as the percentage of cells; Control, n = 8 mice; Lyve1^{ΔCSF1R}, n = 9; *P < 0.0001. Scale bar, 100 μm. **h**, Representative images of podoplanin-stained pancreas tissue and quantification of podoplanin$^+$ area from control or Lyve1^{ΔCSF1R} mice as in **g**; control, n = 8 mice; Lyve1^{ΔCSF1R}, n = 9, *P < 0.0360. **i**, Flow cytometry plots of podoplanin$^+$ pancreas fibroblasts from control and Lyve1^{ΔCSF1R} mice as in **g**. **j**, Density of pancreas podoplanin$^+$ fibroblasts and PDGFRa$^+$ fibroblasts from control and Lyve1^{ΔCSF1R} mice as in **g**; n = 6 mice per group, *P = 0.0411 in podoplanin analysis and *P = 0.0043 in PDGFRa analysis. Data are presented as the mean ± s.e.m. unless otherwise indicated. NS, not significant; *P < 0.05. For comparisons between two groups, Student's two-tailed t-test was used.

CSF1Ab-CLD mice had a >50% reduction in the number of podoplanin$^+$ fibroblasts compared to IgG-PBS mice (Fig. 6b–d). Together, these data suggest that TRMs may impact recovery from pancreatitis by promoting stromagenesis.

To profile how TRMs were involved in driving the fibrotic response during pancreatitis, we examined the changes in fibroblast and ECM deposition during pancreatitis progression. CSF1Ab-CLD or IgG-PBS mice were treated with cerulein for 3, 7 and 17 d. CSF1Ab-CLD mice had reduced numbers of podoplanin$^+$ fibroblasts compared to IgG-PBS mice at all timepoints (Fig. 6d and Extended Data Fig. 8a). The ECM molecule fibronectin was reduced at early timepoints (days 3 and 7 after cerulein injections), but markedly reduced at day 17 compared to IgG-PBS control (Extended Data Fig. 8a). In the absence of pancreatitis, we observed no difference in podoplanin$^+$ fibroblasts between CSF1Ab-CLD and IgG-PBS mice (Extended Data Fig. 8b,c). Flow cytometry indicated the total number of podoplanin$^+$ fibroblasts was markedly increased in IgG-PBS mice, but not in CSF1Ab-CLD mice during pancreatitis (Fig. 6e,f). Four distinct subsets of fibroblasts, including Ly6C$^+$ inflammatory fibroblasts (iFibs), MHCII$^+$ antigen-presenting fibroblasts (apFibs), αSMA$^+$ myofibroblasts (myFibs) and PDGFRα$^+$ fibroblasts (Extended Data Fig. 8d) have been described in homeostatic pancreas and PDAC[37,38]. Of these, we detected an increase in the number of Ly6C$^+$ and PDGFRα$^+$ fibroblasts in IgG-PBS mice, but not in cerulein-treated CSF1Ab-CLD mice (Fig. 6e,f and Extended Data Fig. 8e).

To test whether LYVE1$^+$ macrophages had a role in the initiation of the fibrotic response, we crossed Lyve1-Cre mice with CSF1R$^{fl/fl}$ mice (hereafter Lyve1^{ΔCSF1R}), to specifically delete the *CSF1R* gene in LYVE1$^+$ cells[18]. Lyve1^{ΔCSF1R} mice treated with cerulein for 7 d had >80% reduction in F4/80$^+$LYVE1$^+$CD163$^+$ TRMs compared to Cre$^-$ littermates (Fig. 6g and Extended Data Fig. 8f), but no change in the number of total F4/80$^+$MHCII$^+$ or LYVE1$^-$ macrophages (Extended Data Fig. 8f). Cerulein-treated Lyve1^{ΔCSF1R} mice had reduced expansion of podoplanin$^+$ fibroblasts and PDGFRα$^+$ fibroblasts compared to cerulein-treated Cre$^-$ littermates, as measured by IHC and flow cytometry (Fig. 6h–j). Notably, we observed no increase in iFibs or a survival difference in cerulein-treated Lyve1^{ΔCSF1R} mice compared to their Cre$^-$ counterparts (Extended Data Fig. 8f,g), suggesting other TRMs could partially compensate. To check the role of MDMs, we treated CCR2-KO and wild-type mice with cerulein for 7 d and found no difference in the number of fibroblasts in the pancreas or in ECM deposition (Extended Data Fig. 8h,i). These data suggest TRMs, including LYVE1$^+$ TRMs, coordinated fibroblast activation and expansion during pancreas injury.

Tissue-resident macrophages shape the tissue-protective fibrotic response

To investigate how TRMs impacted fibroblast phenotype, we performed scRNA-seq on sorted podoplanin$^+$ fibroblasts from CSF1Ab-CLD and IgG-PBS mice treated with cerulein by six hourly i.p. injections every other day for 1 week. Uniform manifold approximation and projection

Fig. 7 | Tissue-resident macrophages shape the tissue-protective fibrotic response. a, UMAP plot of pancreas podoplanin$^+$ fibroblasts sorted from IgG + PBS or CSF1Ab + CLD mice rested for 10 d then administered six hourly i.p. injections of Cer every other day for 1 week. **b**, UMAP plots displaying *Pdpn*, *Pdgfra*, *Ly6c1*, *Acta2* and *Col8a1* expression in podoplanin$^+$ pancreas fibroblasts of IgG + PBS and CSF1Ab + CLD mice as in **a**. **c**, UMAP plot showing the classification of fibroblast clusters into Ly6C$^+$ iFib, αSMA$^+$ myFib and MHCII$^+$ apFib subtypes in pancreas podoplanin$^+$ fibroblasts of IgG + PBS and CSF1Ab + CLD mice as in **a**. **d**, UMAP plot of pancreas podoplanin$^+$ fibroblasts from IgG + PBS or CSF1Ab + CLD mice as in **a**. **e**, Heat map displaying NES of gene sets significantly enriched across podoplanin$^+$ fibroblast subtypes (as in **c**) comparing IgG + PBS to CSF1Ab + CLD samples. **f**, Dot plot of DEGs upregulated in podoplanin$^+$ fibroblasts from IgG + PBS mice or CSF1Ab + CLD-treated mice as in **a**. **g**, Heat maps displaying relative importance of network centrality measures for sender (ligand signals) and receiver (receptors) across macrophage clusters from Flt3-YFP mice treated with Cer by six hourly i.p. injections every other day for 1 week (Fig. 3c) and fibroblast clusters as in **a** for PDGF, CCL, CSF1, VCAM and GAS signaling pathway networks from CellChat analysis[49]. **h**, Violin plots showing expression

of PDGF signaling pathway genes *Pdgfa*, *Pdgfb*, *Pdgfc*, *Pdgfra* and *Pdgfrb* across macrophage and fibroblast clusters as in **g**. **i**, Representative images of pancreas tissue stained with podoplanin or fibronectin from mice injected i.p. with Veh or PDGFRi once per day along with six hourly Cer i.p. injections every other day for 1 week. Scale bars, 100 μm. **j**, Quantification of podoplanin$^+$ and fibronectin$^+$ area in pancreas tissue of mice treated with Veh or PDGFRi and cerulein as in **i**; Veh, n = 7 mice; PDGFRi, n = 8 mice; *P = 0.0205 in podoplanin analysis and *P = 0.0140 in fibronectin analysis. **k**, Flow cytometry of podoplanin$^+$ fibroblasts and density of PDGFRa$^+$ fibroblasts from mice treated with Veh or PDGFRi along with Cer as in **i**; n = 7 mice per group and *P = 0.0175. **l**, Body weight measurement and Kaplan–Meier survival curve in mice treated with Veh or PDGFRi along with 10 μg per day Cer delivered by peritoneal osmotic pumps. Measurements started on the day of osmotic pump implantation; n = 10 mice per group, *P < 0.0001 comparing vehicle and PDGFRi in survival curve. Data are presented the mean ± s.e.m. unless otherwise indicated. *P < 0.05. For comparisons between two groups, Student's two-tailed t-test was used, except for **f**, where Bonferroni correction was used, and **e**, where FDR was used.

(UMAP) clustering resulted in ten distinct clusters that broadly fit into the iFib (based on the expression of *Ly6c1* and *Clec3b*), myFib (*Acta2*, *Col8a1*, *Cxcl14*) and apFib (*H2-Ab1*, *Cd74* and *Slpi*) subsets (Fig. 7a–c and Supplementary Table 3)[37,38]. DEG and GSEA analyses indicated *Ly6c1*+ iFibs from IgG-PBS mice were enriched in gene sets related to ECM production and organization and collagen production, while CSF1Ab-CLD *Ly6c1*+ iFibs were enriched in interferon responses and NF-κB signaling, which are known drivers of pancreatitis severity[39,40] (Fig. 7d,e and Supplementary Table 4). Enrichment in these gene sets was also detected in *Acta2*+ myFibs and *H2-Ab1*+ apFibs (Fig. 7e,f). Fibroblasts sorted from pancreas of IgG-PBS + vehicle (steady-state) mice clustered separately from cerulein-treated IgG-PBS or CSF1Ab-CLD fibroblasts, while cerulein-treated IgG-PBS fibroblasts upregulated collagen and ECM

genes more than cerulein-treated CSF1Ab-CLD fibroblasts (Extended Data Fig. 9a,d). This suggests that fibroblasts upregulate genes related to collagen and ECM in the presence of TRMs, but are reduced in number and express genes linked to an inflammatory phenotype rather than protective fibrosis genes, in the absence of TRMs.

Next, to identify TRM–fibroblast signaling molecules, we merged macrophage and fibroblast single-cell datasets and queried LYVE1hi CX3CR1lo MHCIIlo TRMs, LYVE1lo CX3CR1hi MHCIIhi TRMs, CCR2hi MDMs and Ly6C+ iFibs, αSMA+ myFibs and MHCII+ apFibs for enriched receptor and ligand genes (Extended Data Fig. 9e,g). We identified 60 pathways with statistical significance across clusters (Extended Data Fig. 9h). Across all pathways between macrophages and fibroblasts, LYVE1hi TRMs had the highest aggregate score (Extended Data Fig. 9g,i),
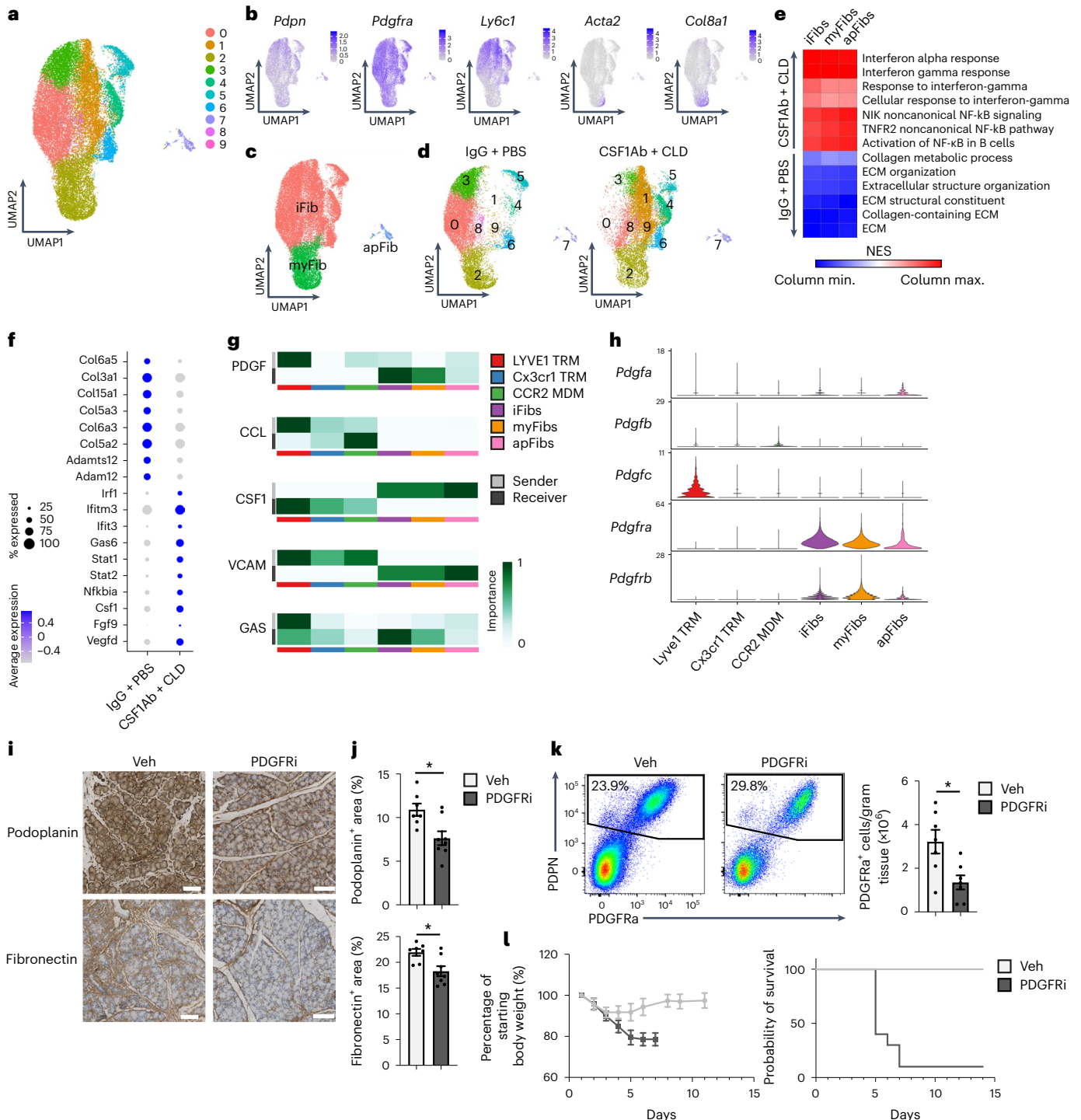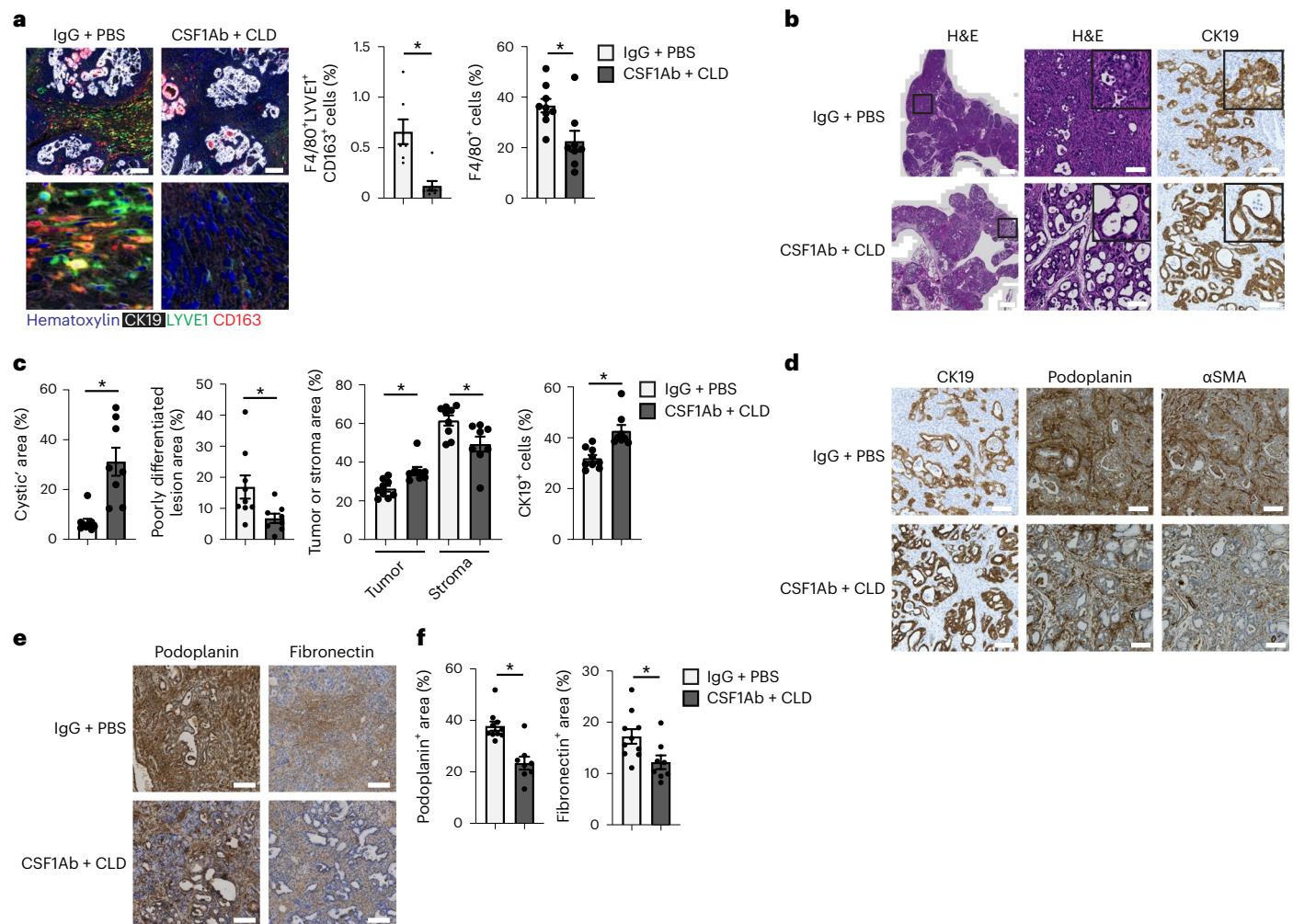
Fig. 8 | Tissue-resident macrophages drive fibrosis and pancreatitis-accelerated pancreatic ductal adenocarcinoma progression.
a, Representative mIHC images of pancreas tissue stained for hematoxylin, CK19, F4/80, LYVE1 and CD163 and quantification of F4/80$^+$LYVE1$^+$CD163$^+$ macrophages and F4/80$^+$ macrophages, displayed as the percentage of cells, from 2.5-month-old p48-Cre LSL-KRAS^{G12D} p53$^{fl/+}$ (KPC) mice treated with IgG + PBS or CSF1Ab + CLD, recovered for 10 d then treated with six hourly i.p. injections of Cer every other day for 5 d; F4/80$^+$LYVE1$^+$CD163$^+$ macrophage analysis: IgG + PBS, n = 7; CSF1Ab + CLD, n = 8 mice; *P = 0.0012; F4/80$^+$ macrophage analysis: IgG + PBS, n = 9; CSF1Ab + CLD, n = 8 mice; *P = 0.0079. Scale bar, 100 μm. **b**, Representative images of pancreas tissue stained for H&E or CK19 from IgG + PBS or CSF1Ab + CLD-treated KPC mice as in **a**. Scale bars, 1 mm (left column) or 100 μM (middle and right columns). **c**, Quantification of tumor area presenting cyst-like appearance, poorly differentiated/high-grade invasive pancreatic tumor lesions, tumor lesions and stromal areas as the percentage of total pancreas area, and CK19$^+$ cells as the percentage of total cells in IgG + PBS or CSF1Ab + CLD KPC mice as in **a**; IgG + PBS, n = 9 mice; CSF1Ab + CLD, n = 8, left to right, *P = 0.0003 for cystic area analysis, *P = 0.0079 for poorly differentiated area analysis, *P = 0.0010 and *P = 0.0152 for tumor and stromal area analysis, and *P = 0.0003 for CK19 analysis. **d**, Representative images of pancreas tissue stained for CK19, podoplanin or αSMA from IgG + PBS or CSF1Ab + CLD KPC mice as in **a**. Scale bars, 100 μm. **e**, Representative images of pancreas tissue from 2-month-old p48-Cre LSL-KRAS^{G12D} p53$^{fl/fl}$ (KPPC) mice treated with IgG + PBS or CSF1Ab + CLD at 1 month of age and rested for 4 weeks. Scale bars, 100 μm. **f**, Quantification of podoplanin$^+$ or fibronectin$^+$ area in KPPC mice treated with IgG + PBS or CSF1Ab + CLD as in **e**. IgG + PBS, n = 10 mice; CSF1Ab + CLD, n = 8, *P = 0.0014 for podoplanin analysis and *P = 0.0205 for fibronectin analysis. Data are presented as the mean ± s.e.m. unless otherwise indicated. *P < 0.05. For comparisons between two groups, Student's two-tailed t-test was used.

suggesting they were likely producing the most signals received by fibroblasts. Among these, PDGF signaling was enriched between LYVE1^{hi} TRMs and both iFibs and myFibs (Fig. 7g). The LYVE1^{hi} cluster had the highest expression of *Pdgfc*, while fibroblasts had high expression *Pdgfra* and *Pdgfrb* (Fig. 7h). Notably, all fibroblast populations produced *Csf1*, which signals through *Csf1r*, expressed by all macrophage clusters (Fig. 7g). To determine if PDGF–PDGFR signaling was required for fibroblast accumulation during pancreatitis, we treated mice with the PDGFR inhibitor imatinib mesylate (hereafter PDGFRi) or vehicle at the time of cerulein administration. PDGFRi-treated mice had reduced podoplanin$^+$ fibroblasts and fibronectin (Fig. 7i,j) and decreased numbers of PDGFRα$^+$ fibroblasts (Fig. 7k), but similar numbers of LYVE1^{hi} and

other TRMs (Extended Data Fig. 9j) compared to vehicle-treated mice. Mice treated with PDGFRi concurrent with cerulein-loaded osmotic pump implantation did not recover body weight and showed 90% lethality (Fig. 7l). These data suggest that fibroblast accumulation during pancreas injury might rely on signals from TRMs, including PDGF–PDGFR signaling.

Tissue-resident macrophages drive fibrosis and pancreatitis-accelerated pancreatic ductal adenocarcinoma progression
To assess whether TRM regulated fibrosis in PDAC, we used three genetic models. These models are driven by pancreas-specific p48-Cre

activation of KRAS^G12D expression either constitutively or under control of doxycycline (iKRAS* mice). Two of the models have Cre-mediated deletion of one p53 allele (hereafter KPC mice) or both p53 alleles (KPPC mice)[41]. KPC mice, aged 2.5 months, were treated with CSF1Ab-CLD and IgG-PBS, rested for 10 d and treated with cerulein by six hourly i.p. injections every other day for 5 d (Extended Data Fig. 10a). Three weeks after cerulein treatment, a timepoint when microscopic carcinomas can be observed in IgG-PBS control mice, CSF1Ab-CLD-treated mice had an 80% reduction in the number of F4/80⁺LYVE1⁺CD163⁺ TRMs compared to IgG-PBS controls (Fig. 8a). By histology, CSF1Ab-CLD-treated KPC mice displayed significantly less high-grade PDAC tissue (Fig. 8b,c), compared to IgG-PBS-treated mice, and instead exhibited well-differentiated cyst-like desmoplastic areas characterized by low stromal desmoplasia and fewer podoplanin⁺ and αSMA⁺ fibroblasts (Fig. 8c,d). These data suggest that TRMs might drive PDAC progression in part through facilitating stromal desmoplasia. In the more aggressive KPPC model, we also observed a reduction in podoplanin and fibronectin staining, and a reduced tumor burden in CSF1Ab-CLD compared to IgG-PBS mice at 2 months of age (Fig. 8e,f)[15]. Finally, to induce depletion of TRMs before KRAS oncogene induction, we treated iKRAS* mice with CSF1Ab-CLD or IgG-PBS, rested for 10 d, then treated with cerulein by i.p. injection for 2 d and administered doxycycline in their drinking water for 3 weeks (Extended Data Fig. 10b)[41,42]. At week 3 after KRAS^G12D induction, CSF1Ab-CLD-treated iKRAS* mice had a significant reduction in F4/80⁺LYVE1⁺CD163⁺ TRMs, as well as reduced premalignant pancreas weight and stromal area compared to IgG-PBS-treated mice (Extended Data Fig. 10c,e). Implantation of tumors in CCR2-KO and wild-type mice resulted in no change in tumor weight, size or podoplanin⁺ fibroblasts (Extended Data Fig. 10f,g). These data indicate that total TRMs facilitate the expansion of the fibrotic stroma during tumor development.

Discussion

Here we showed that a substantial portion of pancreas macrophages were embryonic derived. TRMs in the pancreas did not rely on continual replenishment from monocytes and displayed distinct transcriptional phenotype and location compared to MDMs. The LYVE1^hiCX3CR1^lo MHCII^lo TRM population expressed gene sets indicative of ECM remodeling and alternative activation. Depletion of the LYVE1^hi subset impacted the accumulation and phenotype of fibroblasts during pancreatitis and diminished the effects of protective fibrosis.

It is not fully understood to what extent macrophage origin versus tissue residence or microenvironment impact their phenotype. Lineage tracing studies have shown monocyte-derived cells can adopt a similar phenotype to TRMs over time[6]. Transcriptional and epigenetic profiling has shown macrophages retain tremendous plasticity, and adoptive transfer of TRMs into a different tissue can cause the reprogramming of up to 70% of all genes[14]. This could align with the preferential localization of LYVE1⁺ TRMs within areas of higher fibrosis, suggesting their role in coordinating fibrosis may be driven by their specific microenvironment within the stroma. Further, pancreas TRMs can be distinguished as LYVE1^hiCX3CR1^loMHCII^lo or LYVE1^loCX3CR1^hiMHCII^hi, in agreement with expression of phenotypic markers in TRMs in fat, lung, mesenteric membranes and other tissues[17–20,43]. Studies on LYVE1^hiMHCII^lo TRMs in the lung, arteries and mesenteric membranes report their involvement in ECM remodeling, and display a strikingly similar transcriptional profile to LYVE1^hiMHCII^lo TRMs in the pancreas.

TRM-driven tissue remodeling also led to distinct outcomes depending on the type of tissue injury. TRM-driven fibrosis was critically important for survival and recovery during pancreatitis through protective effects that limited tissue damage. It is thought that pancreatic stellate cell (PSC) activation is critical for recovery following inflammatory injury, both by providing growth factors and possibly driving ductal cell proliferation and regeneration[26,27]. PSC activation for wound healing must, however, be transient. In a chronic setting, prolonged PSC activation is detrimental and can induce extensive fibrosis, which can interfere with pancreas function[23,27]. Our study was limited to acute pancreatitis, where inflammation resolves upon cerulein withdrawal, but it would be important to understand how TRM–fibroblast interactions change in a chronic inflammation setting.

Similar to chronic pancreatitis, tumors involve prolonged inflammation and wound healing responses. We showed that TRM-driven fibrosis was co-opted by tumors to promote tumor growth. While still debated, studies have reported that fibrosis, and even macrophage-induced fibrosis, can play a tumor-supportive role[18,29,44,45]. Fibrotic pathologies have been linked to higher risk of cancer, with chronic pancreatitis being a risk factor for PDAC[46,47]. TRMs have also been reported to support tumor growth through other mechanisms. In lung adenocarcinoma, TRMs coordinate regulatory T cell responses and, when depleted, tumors grow more slowly[21]. In metastatic ovarian cancer models, TRMs promote tumor cell growth and metastatic spreading[18,48]. While the pro-tumor mechanisms of TRMs vary by tumor model, most TRMs display an alternative-activation phenotype and secrete growth factors and cytokines to either directly or indirectly promote tumor progression.

MDMs were reported to promote inflammation and tissue damage during pancreatitis[25]. Our transcriptional profiling indicated the upregulation of inflammatory pathways in MDMs, but we were not able to detect a functional outcome by targeting them. CCR2-KO mice showed no changes in ADM, tissue damage or mouse survival, perhaps due to CCR2-independent mechanisms by which inflammatory macrophages could accumulate. In summary, our study demonstrates that LYVE1^hi TRMs expand in number to help coordinate a fibrotic response critical in protecting the exocrine pancreas from inflammatory damage, but this program is co-opted by tumors to support their growth.

Online content

Any methods, additional references, Nature Portfolio reporting summaries, source data, extended data, supplementary information, acknowledgements, peer review information; details of author contributions and competing interests; and statements of data and code availability are available at https://doi.org/10.1038/s41590-023-01579-x.

References

1. Ginhoux, F. et al. Fate mapping analysis reveals that adult microglia derive from primitive macrophages. *Science* **330**, 841–845 (2010).
2. Hoeffel, G. et al. C-Myb⁺ erythro-myeloid progenitor-derived fetal monocytes give rise to adult tissue-resident macrophages. *Immunity* **42**, 665–678 (2015).
3. Epelman, S. et al. Embryonic and adult-derived resident cardiac macrophages are maintained through distinct mechanisms at steady state and during inflammation. *Immunity* **40**, 91–104 (2014).
4. Schulz, C. et al. A lineage of myeloid cells independent of Myb and hematopoietic stem cells. *Science* **336**, 86–90 (2012).
5. Hashimoto, D. et al. Tissue-resident macrophages self-maintain locally throughout adult life with minimal contribution from circulating monocytes. *Immunity* **38**, 792–804 (2013).
6. Liu, Z. et al. Fate mapping via Ms4a3-expression history traces monocyte-derived cells. *Cell* **178**, 1509–1525 (2019).
7. Yona, S. et al. Fate mapping reveals origins and dynamics of monocytes and tissue macrophages under homeostasis. *Immunity* **38**, 79–91 (2013).
8. Bain, C. C. et al. Long-lived self-renewing bone marrow-derived macrophages displace embryo-derived cells to inhabit adult serous cavities. *Nat. Commun.* **7**, ncomms11852 (2016).
9. Ginhoux, F. & Guilliams, M. Tissue-resident macrophage ontogeny and homeostasis. *Immunity* **44**, 439–449 (2016).

10. Calderon, B. et al. The pancreas anatomy conditions the origin and properties of resident macrophages. *J. Exp. Med.* **212**, 1497–1512 (2015).

11. Bain, C. C. et al. Constant replenishment from circulating monocytes maintains the macrophage pool in the intestine of adult mice. *Nat. Immunol.* **15**, 929–937 (2014).

12. Kim, K.-W. et al. MHC II+ resident peritoneal and pleural macrophages rely on IRF4 for development from circulating monocytes. *J. Exp. Med.* **213**, 1951–1959 (2016).

13. Loyher, P.-L. et al. Macrophages of distinct origins contribute to tumor development in the lung. *J. Exp. Med.* **215**, 2536–2553 (2018).

14. Lavin, Y. et al. Tissue-resident macrophage enhancer landscapes are shaped by the local microenvironment. *Cell* **159**, 1312–1326 (2014).

15. Zhu, Y. et al. Tissue-resident macrophages in pancreatic ductal adenocarcinoma originate from embryonic hematopoiesis and promote tumor progression. *Immunity* **47**, 323–338 (2017).

16. Ginhoux, F. & Jung, S. Monocytes and macrophages: developmental pathways and tissue homeostasis. *Nat. Rev. Immunol.* **14**, 392–404 (2014).

17. Chakarov, S. et al. Two distinct interstitial macrophage populations coexist across tissues in specific subtissular niches. *Science* **363**, eaau0964 (2019).

18. Zhang, N. et al. LYVE1+ macrophages of murine peritoneal mesothelium promote omentum-independent ovarian tumor growth. *J. Exp. Med.* **218**, e20210924 (2021).

19. Lim, H. Y. et al. Hyaluronan receptor LYVE-1-expressing macrophages maintain arterial tone through hyaluronan-mediated regulation of smooth muscle cell collagen. *Immunity* **49**, 326–341 (2018).

20. Dick, S. A. et al. Three tissue resident macrophage subsets coexist across organs with conserved origins and life cycles. *Sci. Immunol.* **7**, eabf7777 (2022).

21. Casanova-Acebes, M. et al. Tissue-resident macrophages provide a pro-tumorigenic niche to early NSCLC cells. *Nature* **595**, 578–584 (2021).

22. Apte, M., Pirola, R. & Wilson, J. The fibrosis of chronic pancreatitis: new insights into the role of pancreatic stellate cells. *Antioxid. Redox Signal.* **15**, 2711–2722 (2011).

23. Klöppel, G., Detlefsen, S. & Feyerabend, B. Fibrosis of the pancreas: the initial tissue damage and the resulting pattern. *Virchows Arch.* **445**, 1–8 (2003).

24. Liou, G.-Y. et al. Macrophage-secreted cytokines drive pancreatic acinar-to-ductal metaplasia through NF-κB and MMPs. *J. Cell Biol.* **202**, 563–577 (2013).

25. Saeki, K. et al. CCL2-induced migration and SOCS3-mediated activation of macrophages are involved in cerulein-induced pancreatitis in mice. *Gastroenterology* **142**, 1010–1020 (2012).

26. Zimmermann, A. Pancreatic stellate cells contribute to regeneration early after acute necrotising pancreatitis in humans. *Gut* **51**, 574–578 (2002).

27. Omary, M. B., Lugea, A., Lowe, A. W. & Pandol, S. J. The pancreatic stellate cell: a star on the rise in pancreatic diseases. *J. Clin. Invest.* **117**, 50–59 (2007).

28. Hosein, A. N., Brekken, R. A. & Maitra, A. Pancreatic cancer stroma: an update on therapeutic targeting strategies. *Nat. Rev. Gastroenterol. Hepatol.* **17**, 487–505 (2020).

29. Chandler, C., Liu, T., Buckanovich, R. & Coffman, L. G. The double edge sword of fibrosis in cancer. *Transl. Res.* **209**, 55–67 (2019).

30. Lerch, M. M. & Gorelick, F. S. Models of acute and chronic pancreatitis. *Gastroenterology* **144**, 1180–1193 (2013).

31. Boyer, S. W., Schroeder, A. V., Smith-Berdan, S. & Forsberg, E. C. All hematopoietic cells develop from hematopoietic stem cells through Flk2/Flt3-positive progenitor cells. *Cell Stem Cell* **9**, 64–73 (2011).

32. Bowman, R. L. et al. Macrophage ontogeny underlies differences in tumor-specific education in brain malignancies. *Cell Rep.* **17**, 2445–2459 (2016).

33. Zhou, D. C. et al. Spatially restricted drivers and transitional cell populations cooperate with the microenvironment in untreated and chemo-resistant pancreatic cancer. *Nat. Genet.* **54**, 1390–1405 (2022).

34. Lee, B. et al. Single-cell sequencing unveils distinct immune microenvironments with CCR6-CCL20 crosstalk in human chronic pancreatitis. *Gut* **71**, 1831–1842 (2021).

35. Yu, J. et al. Liver metastasis restrains immunotherapy efficacy via macrophage-mediated T cell elimination. *Nat. Med.* **27**, 152–164 (2021).

36. Serbina, N. V. & Pamer, E. G. Monocyte emigration from bone marrow during bacterial infection requires signals mediated by chemokine receptor CCR2. *Nat. Immunol.* **7**, 311–317 (2006).

37. Elyada, E. et al. Cross-species single-cell analysis of pancreatic ductal adenocarcinoma reveals antigen-presenting cancer-associated fibroblasts. *Cancer Discov.* **9**, 1102–1123 (2019).

38. Öhlund, D. et al. Distinct populations of inflammatory fibroblasts and myofibroblasts in pancreatic cancer. *J. Exp. Med.* **214**, 579–596 (2017).

39. Manohar, M., Verma, A. K., Venkateshaiah, S. U., Sanders, N. L. & Mishra, A. Pathogenic mechanisms of pancreatitis. *World J. Gastrointest. Pharm. Ther.* **8**, 10–25 (2017).

40. Habtezion, A. Inflammation in acute and chronic pancreatitis. *Curr. Opin. Gastroenterol.* **31**, 395–399 (2015).

41. Guerra, C. et al. Chronic pancreatitis is essential for induction of pancreatic ductal adenocarcinoma by K-Ras oncogenes in adult mice. *Cancer Cell* **11**, 291–302 (2007).

42. Collins, M. A. et al. Oncogenic Kras is required for both the initiation and maintenance of pancreatic cancer in mice. *J. Clin. Invest.* **122**, 639–653 (2012).

43. Gibbings, S. L. et al. Three unique interstitial macrophages in the murine lung at steady state. *Am. J. Respir. Cell Mol. Biol.* **57**, 66–76 (2017).

44. DeNardo, D. G. & Ruffell, B. Macrophages as regulators of tumour immunity and immunotherapy. *Nat. Rev. Immunol.* **19**, 369–382 (2019).

45. Jiang, H. et al. Targeting focal adhesion kinase renders pancreatic cancers responsive to checkpoint immunotherapy. *Nat. Med.* **22**, 851–860 (2016).

46. Vujasinovic, M. et al. Risk of developing pancreatic cancer in patients with chronic pancreatitis. *J. Clin. Med.* **9**, 3720 (2020).

47. Lowenfels, A. B. et al. Pancreatitis and the risk of pancreatic cancer. *N. Engl. J. Med.* **328**, 1433–1437 (1993).

48. Etzerodt, A. et al. Tissue-resident macrophages in omentum promote metastatic spread of ovarian cancer. *J. Exp. Med.* **217**, e20191869 (2020).

49. Jin, S. et al. Inference and analysis of cell–cell communication using CellChat. *Nat. Commun.* **12**, 1088 (2021).

Methods

Mouse models

The following mouse models were purchased from Jackson Laboratories: CCR2-KO, Rosa26-LSL-eYFP and Csf1r-mer-iCre-mer. Lyve1-Cre;CSF1R$^{fl/fl}$ (Lyve1$^{\Delta CSF1R}$) mice were a gift from G. Randolph at Washington University in St. Louis. LSL-tdTomato mice in the FVB/NJ background were a gift from G. Longmore at Washington University in St. Louis, and were crossed to Csf1r-mer-iCre-mer for lineage tracing studies. Flt3-Cre mice were a gift from T. Boehm at the Max Planck Institute, and were crossed to Rosa26-LSL-eYFP mice. For Flt3-Cre;Rose26-LSL-eYFP experiments, male mice were used between the ages of 8 and 16 weeks. All other experiments were performed on both male and female mice between the ages of 8 and 16 weeks. Mice were maintained in the Laboratory for Animal Care barrier facility at the Washington University School of Medicine under a 12-h light–dark cycle. Washington University School of Medicine Institutional Animal Studies Committee approved all animal studies. Survival endpoints were scored when mice lost >15% body weight or tumors reached >1.8 cm in diameter by palpation.

Mouse tumor models

KPC mice (p48-Cre;LSL-KRAS^{G12D};p53$^{fl/+}$) used in these studies have been previously described. They were backcrossed to C57BL/6 mice and tested for congenic markers. iKRAS* mice (Pft1a-Cre;LSL-rtTa; TetO-KRAS^{G12D}) were a kind gift from M. Pasca di Magliano, and have been previously characterized. Briefly, Kras^{G12D} expression was induced by administration of doxycycline in drinking water at a concentration of 0.5 mg ml^{-1}, supplemented with 3% sucrose (wt/vol). Upon start of doxycycline, mice were treated with acute cerulein on two consecutive days, injecting 100 µg per kg body weight of cerulein every hour for 6 h each day. Doxycycline administration was continued for 3 weeks, replacing drinking water every 3 d. The KPC-1 cell line was derived from a 2.2-month-old KPPC mouse (p48-Cre;LSL-KRAS^{G12D};p53$^{fl/fl}$), and grown on collagen-coated tissue culture flasks for <12 generations. To establish orthotopic pancreas KPC tumor models, Flt3-YFP or C57BL/6 mice were implanted with 100,000 KPC-1 cells in 5 µl serum-free DMEM/F-12 and 45 µl Cultrex (Trevigen) by injecting cells directly into the pancreas.

For lung tumors, the KPL86 cell line was derived from lung tissues of the 9-month-old *Kras*$^{LSL-G12D}$/*p53*$^{flox/+}$ mouse treated with adenovirus-delivered Cre recombinase. Cells were grown on collagen-coated tissue culture flasks for <10 passages. To establish orthotopic non-small-cell lung cancer models, 1,000,000 KPL86 cells in 100 µl of PBS (Trevigen) were retro-orbitally injected into 8- to 12-week-old Flt3-YFP mice.

For liver metastasis of PDAC cells, hemispleen injection of 500,000 KPC-2 (or 'KP2') tumor cells was performed using an adapted procedure from published studies[50,51]. The KP2 cell line was derived from pancreatic tumors of a 6-month-old p48-CRE+/LSL-KRAS^{G12D}/p53$^{flox/+}$ mouse, and tumor cells additionally were modified to express mCherry and click beetle red luciferase. To implant cells in the liver, the mice were anesthetized under continuously monitored isoflurane, and the spleen was exteriorized from the peritoneal cavity under sterile conditions through a left flank laparotomy. The spleen was ligated using medium titanium Horizon ligation clips (Teleflex) and divided in half. A tumor single-cell suspension in sterile PBS (100 µl), followed by 150 µl of sterile PBS flush, was injected into the inferior pole of the spleen with a 30-gauge needle (BD), monitoring for blanching of the spleen parenchyma and splenic vein to ensure injection efficacy. Once the cells and PBS flush were injected, the splenic vein was ligated, and the inferior pole of the spleen was excised. Once hemostasis was ensured, the peritoneum was closed with 5-0 ligature (Ethicon), and the skin was closed with the AutoClip system (Braintree Scientific). Mice were post-operatively monitored and managed according to Institutional Animal Care and Use Committee guidelines for survival surgery. Livers were collected at day 14 for cell sorting and scRNA-seq analysis.

Human samples

Human PDAC (with adjacent non-tumor 'normal' pancreatic tissue) and pancreatitis (with adjacent 'normal' pancreatic tissue) samples were obtained from consenting individuals diagnosed at Barnes-Jewish Hospital. The studies described were approved by the Washington University Institutional Review Board under protocol numbers 201704078 and 201908148. Adjacent healthy pancreas was identified by a pathologist using H&E-stained slides.

Experimental pancreatitis

Acute pancreatitis was induced in mice by administering six hourly i.p. injections of cerulein at a dosage of 100 µg per kg body weight given every other day for 1 week.

For severe acute pancreatitis via osmotic pump delivery of cerulein, osmotic pumps (Alzet Osmotic Pumps) were loaded with 100 µl of concentrated cerulein (8 µg cerulein per day was loaded with 1.33 mg ml^{-1} and 10 µg cerulein per day was loaded with 1.67 mg ml^{-1}). Pumps were then implanted into the peritoneal cavity of mice, and body weight was monitored every day for up to 14 d.

Macrophage depletion

TRMs were depleted with a combination of CSF1 neutralizing antibodies and CLDs. Eight- to twelve-week-old FVB/NJ mice were treated with two doses of CSF1 antibody (BioXcell, 5A1, 1 mg and 0.5 mg on days −14 and −11, respectively), followed by two doses of CLDs (Liposoma, 200 µl each dose) on days −13 and −10. Mice were then allowed to recover for 10 d to allow monocytes and MDMs to reconstitute. On day 0, mice were either treated with cerulein by i.p. injection (described above) or implanted with osmotic pump to deliver cerulein.

Similarly, KPC mice were treated with two doses of CSF1 antibody (1 mg and 0.5 mg) separated by 2 d and starting at 10 weeks of age. On subsequent days after CSF1 antibody treatment, mice were injected with 100 µl of CLDs. Mice were then allowed to recover for ~2 weeks, then given brief cerulein treatment starting at 12 weeks of age by giving six hourly injections of 100 µg per kg body weight cerulein every other day for 5 d. Following cerulein, tumors were allowed to grow for ~3 weeks and mice were euthanized at 15 weeks of age. KPPC mice were similarly treated with two doses of CSF1 antibody (both 0.5 mg) and two doses of CLDs (100 µl each) starting at 1 month of age, as previously described[52]. Tissue was then taken and analyzed at 2 months of age.

iKRAS* mice were treated with a similar regimen of two doses of CSF1 antibody (1 mg and 0.5 mg) 14 and 11 d before starting doxycycline administration. Following CSF1 antibody treatment, mice were injected with CLDs (100 µl) on subsequent days. After CSF1 antibody and clodronate treatment, mice were allowed to recover for 10 d, after which doxycycline was given in drinking water (0.5 mg ml^{-1} with 3% sucrose replaced every 3 d, as above) for ~3 weeks. Additionally, on days 0 and 1, iKRAS* mice were treated with acute cerulein (100 µg per kg body weight) by six hourly injections.

Lineage tracing

For lineage tracing of embryonically derived macrophages, timed breeding pairs were set up by crossing Csf1r-mer-iCre-mer mice with Rosa26-LSL-tdTomato mice (both on FVB/NJ background). The embryonic timeline was estimated by observation of the vaginal plug, with 12:00 on the day of plug formation being 0.5 days post coitum. Pregnant mice were then treated with tamoxifen (75 µg per gram body weight) supplemented with progesterone (37.5 µg per gram body weight) dissolved in corn oil at ~9.5 days post coitum. Offspring of tamoxifen-pulsed mice were then treated with vehicle or acute cerulein (as described above) at 6 weeks of age and euthanized for fate mapping analyses.

For lineage tracing of resident macrophages, adult Cx3cr1-CreERT2;LSL-tdTomato and Csf1r-mer-iCre-mer;LSL-tdTomato mice were pulsed with tamoxifen (75 mg per kg body weight) dissolved in

corn oil on five consecutive days. Mice were then allowed a chase period of 3–10 weeks, or until blood monocytes lost tdTomato labeling. Following the chase period, mice were treated with vehicle or acute cerulein as described above, then euthanized for flow cytometry or IHC analyses.

Parabiosis

Parabiotic pairs were established based on previously described protocols[52,53]. Briefly, age-matched and weight-matched female CD45.2+ and CD45.1+ mice were surgically joined. Mice were injected with Buprenex (buprenorphine) subcutaneously after surgery. Sulfatrim was continuously added in drinking water for 10 d after surgery to minimize infections in surgical wounds. Mice were separated and perfused with PBS containing 0.2% heparin. Single-cell suspensions from tissues were stained with antibodies for flow cytometry analyses 6 weeks after the establishment of parabiosis.

PDGFR inhibition with imatinib mesylate

Mice were treated once daily with i.p. injection of 100 mg per kg body weight imatinib mesylate (MCE, HY-50946). Imatinib was dissolved in 10% DMSO in PBS, then diluted at a 1:10 ratio for a final concentration of 100 mg per kg body weight in 1% DMSO solution. Concurrent with imatinib treatment, mice were either treated with standard i.p. injection of cerulein for flow cytometry and histology experiments, or implanted with osmotic pumps loaded with 1.67 mg ml^{-1} cerulein to deliver 10 µg per day (as described above).

Mouse tissue isolation and flow cytometry

Mice were euthanized by cardiac perfusion with ~10–15 ml PBS-heparin under isoflurane anesthesia. Pancreas or tumor tissue was then isolated, minced with scissors, and digested in ~15–25 ml DMEM with 2 mg ml^{-1} Collagenase A and 1× DNase I for either 15 min (steady-state pancreas and cerulein-treated pancreas) or 25 min (tumor tissue) at 37 °C with constant stirring. Digestion buffer was quenched with 3 ml FBS and filtered through 100-µm Nylon mesh, pelleted by centrifugation (2,000 r.p.m. for 5 min) and resuspended in FACS buffer (1% BSA in PBS). Brain tissue was minced and triturated through 40-µm Nylon mesh and resuspended in FACS buffer to obtain a single-cell suspension.

Cell suspensions were then blocked with rat anti-mouse CD16/CD32 antibodies for 10 min on ice, pelleted by centrifugation, and stained with fluorophore-conjugated extracellular antibodies for 25 min on ice. For samples with endogenous fluorescent protein labeling, cells were then washed twice with FACS Buffer, then run on a BD Fortessa X20 immediately. For unlabeled cells, samples were washed twice following antibody staining, fixed with BD Fixation Buffer for 30 min on ice, washed and resuspended in FACS buffer. Fixed samples were stored at 4 °C and run on a BD Fortessa X20 within 2 weeks. For samples requiring intracellular staining, cells were washed following extracellular staining, and stained using eBioscience FoxP3 Transcription Factor Staining Kit according to the manufacturer's instructions.

To quantify proliferating cells in Flt3-YFP mice, tissue was digested and extracellular staining was conducted as described above. Cells were then fixed in 4% paraformaldehyde for 10 min on ice, then permeabilized in ice-cold 70% ethanol for 3 h, and stained with Ki67 antibody diluted in FACS buffer for 20 min on ice. Cells were then washed twice and immediately run on a BD Fortessa X20.

To quantify blood monocytes, 100 µl blood was obtained by cardiac puncture before perfusions and deposited into PBS-heparin. Blood was then pelleted by centrifugation, resuspended in 5 ml red blood cell lysis buffer for 10 min at room temperature, cells pelleted by centrifugation, then stained with fluorophore-conjugated antibodies for 25 min on ice. Cells were then fixed in BD Fixation Buffer for 30 min on ice, washed twice with FACS buffer, and stored at 4 °C and run on a BD Fortessa X20 within 2 weeks. For experiments requiring blood quantification before mice being euthanized, blood was obtained by tail vein bleeding, resuspended in RBS lysis buffer, stained with extracellular antibodies as described above.

Fluorescence-activated cell sorting

Single-cell suspensions were obtained as described above. Cells were then resuspended in FACS buffer containing CD16/CD32 antibodies to block for 10 min on ice, pelleted by centrifugation, then resuspended in fluorophore-conjugated antibodies, stained for 25 min on ice, then washed with FACS buffer. Cells were then immediately sorted on a FACSAria II (BD Biosciences).

For homeostatic pancreas, pancreatitis and pancreatic tumors, live macrophages (CD45+CD11b+CD3−CD19−B220−SiglecF−Ly6G−Ly6 C−7AAD−F4/80+MHCII$^{hi/lo}$) were sorted. For bulk RNA-seq analyses, Flt3-YFP-positive and Flt3-YFP-negative macrophages were sorted directly into RNA lysis buffer (Omega Biotek) and RNA isolated using EZNA Kit (Omega Biotek). For scRNA-seq, cells were sorted into FACS buffer, and library preparation was conducted as described below.

Liver single-cell suspensions were obtained as described above. Cells were then resuspended in anti-CD45 magnetic beads (BD Biosciences), incubated for 15 min on ice, washed in FACS buffer, and applied to an LS magnetic column to enrich for CD45+ cells. Following magnetic isolation, cells were spun down, resuspended in fluorophore-conjugated antibodies, stained for 25 min on ice, washed with FACS buffer, then immediately sorted. Flt3-YFP-positive and Flt3-YFP-negative liver macrophages were sorted (CD45+CD11b+CD3− CD19−B220−SiglecF−Ly6G−7AAD−) into FACS buffer, then scRNA-seq library preparation was conducted as described below.

Lung single-cell suspensions were obtained as described above. Cells were then resuspended in FACS buffer containing CD16/CD32 antibodies to block for 10 min on ice, pelleted by centrifugation, then resuspended in fluorophore-conjugated antibodies, stained for 25 min on ice, then washed with FACS buffer. Cells were then immediately sorted on a FACSAria II (BD Biosciences). Flt3-YFP-positive and Flt3-YFP-negative macrophages were sorted (CD45+CD3−CD19−B220− 7AAD−CD11b+CD11c$^{hi/lo}$F4/80+) into FACS buffer, then scRNA-seq library preparation was conducted as described below.

For fibroblasts, homeostatic pancreas or cerulein-treated pancreas tissue was taken, and single-cell suspensions were isolated as described above. Cells were then resuspended in FACS buffer containing CD16/CD32 antibodies to block for 10 min on ice, pelleted by centrifugation, then resuspended in fluorophore-conjugated antibodies, stained for 25 min on ice, then washed with FACS buffer. Cells were then immediately sorted on a FACSAria II (BD Biosciences). Total fibroblasts were sorted (CD45−EpCAM−CD31−PDPN+) into FACS buffer, then scRNA-seq library preparation was conducted as described below.

After cells were sorted into FACS buffer, they were pelleted by centrifugation, resuspended in 0.04% BSA in PBS, and cell counts were obtained. scRNA-seq library preparation was then conducted by the Genome Technology Access Center at Washington University. Briefly, cells from each sample were encapsulated into droplets, and libraries were prepared using Chromium Single Cell 3′ v3 Reagent kits according to the manufacturer's protocol (10x Genomics). The generated libraries were sequenced by a NovaSeq 6000 sequencing system (Illumina) to an average of 50,000 mean reads per cell. Cell Ranger mkfastq pipeline (10x Genomics) was used to demultiplex Illumina base call files to FASTQ files. Afterward, fastq files from each sample were processed with Cell Ranger counts and aligned to the mouse mm10 reference genome (Cell Ranger v4.0.0, 10x Genomics, mouse reference mm10-2020-A from https://cf.10xgenomics.com/supp/cell-exp/refdata-gex-mm10-2020-A.tar.gz) to generate feature barcode matrix.

Mouse bulk RNA-seq analysis

Pancreas macrophages were sorted as described above, directly into TRK Lysis buffer (Omega Bio-Tek). RNA was isolated by E.Z.N.A. Total

RNA isolation kit according to the manufacturer's recommendations (Omega Bio-Tek). Following quality control by bioanalyzer, libraries were prepared using the Clontech SMARTer kit (Takara Bio) at the Washington University Genome Technology Access Center (GTAC). Libraries were then indexed, pooled and sequenced on an Illumina HiSeq 3000 (Illumina). Illumina's bcl2fastq software was then used for basecalling and demultiplexing. Reads were then aligned to the Ensembl release 76 top-level assembly with STAR version 2.0.4b, and gene counts were derived from the number of uniquely aligned unambiguous reads by Subread:featureCount version 1.4.5. Gene counts were then imported into Edge in R, and TMM normalization size factors were calculated to adjust for differences in library size. Limma and voomWithQualityWeights were then used to calculate weighted likelihoods based on the observed mean–variance relationship of every gene and sample. Differential expression analysis was then performed to analyze for differences between Flt3-YFP lineages and results filtered by Benjamini–Hochberg FDR-adjusted P values less than or equal to 0.05. Global perturbations in known Gene Ontology (GO) terms and KEGG pathways were detected using GAGE to test for changes in expression of reported $\log_2$ fold changes reported by Limma in each term versus background $\log_2$ fold changes of all genes outside the respective term. GSEA was also performed using GO terms, KEGG pathways, Reactome and MSigDB gene sets with Benjamini–Hochberg FDR < 0.05. DEGs and gene sets were displayed using pHeatmap or the Phantasus online tool (Artyomov; https://artyomovlab.wustl.edu/phantasus/).

Mouse single-cell RNA-seq analysis

The filtered feature barcode matrix from each sample was then loaded into Seurat as Seurat objects (Seurat v3). For each Seurat object, genes that were expressed in less than three cells and cells that expressed less than 1,000 or more than 8,000 genes, were excluded. Cells with greater than 10% mitochondrial RNA content were also excluded, resulting in between 2,297 and 17,880 cells, as indicated in Supplementary Table 1. SCTransform with default parameters was used on each individual sample to normalize and scale the expression matrix against the sequence depths and percentages of mitochondrial genes[54]. Principle component analysis (PCA) was performed (function RunPCA). A UMAP dimensional reduction was performed on the scaled matrix using the first 25 PCA components to obtain a two-dimensional representation of cell states. Then, these defined 25 dimensionalities were used to refine the edge weights between any two cells based on Jaccard similarity (FindNeighbors), and were used to cluster cells through FindClusters functions.

To characterize clusters, the FindAllMarkers function with a logfold threshold of 0.25 and minimum 0.25-fold difference and MAST test were used to identify signatures alone with each cluster. For macrophage/monocyte samples, the macrophage/monocytes clusters were selected, and the top 3,000 variable features were recalculated to recluster to a higher resolution. Macrophages were selected based on clusters with high expressions of known macrophage marker genes, including *Csf1r*, *C1qa* and *C1qb*, and confirmed by the absence of *Cd3e*, *Ms4a1*, *Krt19*, *Zbtb46* and *Flt3*, and further confirmed by identifying DEGs associated with potential macrophage clusters, when compared to known macrophage-specific marker genes. For fibroblast samples, the fibroblast clusters were selected and similarly reclustered. Fibroblasts were selected based on clusters with high expression of known fibroblast marker genes, including *Pdpn*, *Pdgfra* and *Col1a1*, and confirmed by the absence of *Krt19*, *Prss2* and *Amy1a*. For GSEA comparisons, the $\log_2$(fold change) of all genes detected with min.pct > 0.1 and past MAST test was used as a ranking metric. GSEA was performed using GO terms, KEGG pathways, Reactome and MSigDB gene sets with Benjamini–Hochberg FDR < 0.05 in ClusterProfiler[55]. For DEGs between the two groups in each library, we filtered genes with a Bonferroni-corrected P value < 0.05 and fold change > 1.2 or < 0.8.

Human single-cell RNA-seq analysis

For the human datasets[33], cells with greater than 15% mitochondrial genes were excluded and cells that expressed less than 500 genes were excluded. SCTransform with default parameters was used on each individual sample to normalize and scale the expression matrix against sequence depth and percentage of mitochondrial genes[54]. Cell cycle scores and corresponding cell cycle phases were then calculated and assigned after SCTransform based on S and G2/M genes (CellCycle Scoring). Differences between the S phase and G2/M phase were then regressed out by SCTransform on individual samples. Variable features were calculated for every sample in the dataset independently and ranked based on the number of samples they were independently identified (SelectIntegrationFeatures). The top 3,000 variable features were then used for PCA (RunPCA). The calculated PCA embedding of each cell was then used as an input for the soft k-means clustering algorithm. Briefly, through iteration, the algorithm designated the cluster-specific centroids and cell-specific correction factors corresponding to batch effects. The correction factors were used to assign cells into clusters until the assignment was stable (RunHarmony). The first 20 PCA components were then used to refine the edge weights between any two cells based on Jaccard similarity (FindNeighbors), and were used to cluster cells through the FindClusters function at a resolution of 0.3, resulting in 24 clusters. To characterize clusters, the FindAllMarkers function with logfold threshold of 0.25 and minimum 0.25-fold difference and MAST test were used to identify signatures alone with each cluster. Macrophage/monocyte clusters were then selected, and the top 3,000 variable features were recalculated to recluster to a higher resolution, resulting in 5,970 total cells and 8 clusters. Macrophages were selected based on clusters with high expressions of known macrophage marker genes, including *CSF1R*, *C1QA*, *C1QB* and *CD68*, and confirmed by the absence of *CD3E*, *MS4A1*, *KRT19* and *CD1C*, and further confirmed by identifying DEGs associated with potential macrophage clusters, when compared to known macrophage-specific marker genes.

Immunohistochemistry and immunofluorescence

Mouse tissues were fixed in 10% formalin overnight at 4 °C, dehydrated through graded ethanol washes of 30% ethanol, 50% ethanol and 70% ethanol for 20 min each. Tissue was then run through a Leica ASP 6025 tissue processor and embedded in paraffin, then sectioned at 6-μm-thick tissue sections. IHC staining was then performed on a Bond Rxm autostainer (Leica Biosystems) according to the manufacturer's recommendations. Briefly, paraffin slides were loaded onto the machine, baked at 60 °C for 15 min, dewaxed and rehydrated, and antigen was retrieved with either citrate or EDTA antigen retrieval solution (Leica Biosystems). Endogenous peroxidase activity was blocked with a peroxide block, and primary antibodies were then applied for 60 min. Either species-specific or biotinylated secondary antibodies were then applied to the slides. Next, either DAB or Fast Red chromogens were applied, followed by hematoxylin counterstain. Slides stained with DAB were then dehydrated through graded ethanols and xylene, and then mounted with Cytoseal XYL (Thermo Fisher). Slides stained with Fast Red were air dried for 15 min and then mounted with Vectamount Permanent Mounting Medium (Vector Laboratories).

Multiplex immunohistochemistry staining

Formalin-fixed paraffin-embedded tissue was sectioned at 6 μm, loaded onto a Bond Rxm autostainer, baked for 60 min at 60 °C, dewaxed and rehydrated. A series of staining was performed with multiple markers as indicated, based on a previously published study[56]. Briefly, slides were first blocked with peroxide block, goat serum block and species-specific F'ab block (Jackson Laboratories), then primary antibodies were incubated for 60 min, followed by species-specific secondary antibodies conjugated to horseradish peroxidase (HRP). For primary antibodies raised in rabbit, Polymer (anti-rabbit poly-HRP, Leica Biosystems) was used as a secondary antibody; for primary antibodies

raised in mouse, Post-Primary (rabbit anti-mouse, Leica Biosystems) secondary was used, followed by Polymer; and for other primary antibodies, biotinylated species-specific secondaries were used, followed by streptavidin-HRP (SA-HRP, Leica Biosystems; anti-rabbit poly-HRP and SA-HRP are provided in Intense R and Polymer Refine Detection Kits respectively, Leica Biosystems). Slides were then chromogenically visualized with AEC (Invitrogen) and counterstained with hematoxylin (Dako). Stained slides were then mounted with Vectamount Aqueous Mounting Medium (Vector Laboratories) and imaged on an Axio Scan. Z1 (Zeiss) at ×20 magnification. Before the next round of staining, coverslips and mounting medium were removed by soaking slides in TBST (1× TBS with 0.05% Tween-20) for several hours, then destained by graded ethanols (50% ethanol, 70% ethanol with 1% HCl, 100% ethanol, 70% ethanol, 50% ethanol and deionized water for 5–10 min each) then loaded onto a Bond Rxm for staining of the next marker. Images were cropped and exported using Zeiss ZEN software (v3.2.0) then analyzed using HALO software (Indica Labs).

Quantification and statistical analysis

The number of mice and statistical tests used are reported in each figure legend. Statistical analyses were performed by GraphPad Prism v9, using an unpaired Student's t-test, analysis of variance (Bonferroni multiple comparisons) or unpaired non-parametric Mann–Whitney U test as appropriate for normality of data. A log rank (Mantel–Cox) test was used for survival experiments. Data are the mean ± s.e.m., unless otherwise noted. $P < 0.05$ was considered statistically significant for all studies; *$P < 0.05$. Mice genotyped as positive for strain-specific alleles were allocated randomly into treatment groups. Littermate controls that were genotyped negative were subsequently allocated randomly into control groups when appropriate. All mice were assigned numbers to allow researchers to be blinded to mouse genotype or treatment group where possible. During data collection by flow cytometry, IHC analysis or pathological grading, mice were only referred to by their number to avoid bias toward genotype or treatment group. Data were then organized according to group or treatment once data collection was complete.

Reporting summary

Further information on research design is available in the Nature Portfolio Reporting Summary linked to this article.

Data availability

Sequencing data are publicly available under Gene Expression Omnibus repository accession numbers GSE196778 (scRNA-seq) and GSE203005 (bulk RNA-seq). Source data are provided with this paper. All other data are available upon request from the corresponding author.

Code availability

No custom code was generated for this study. Code used to generate figures is available upon request from the corresponding author.

References

50. Soares, K. C. et al. A preclinical murine model of hepatic metastases. *J. Vis. Exp.* **27**, 51677 (2014).
51. Lee, J. W. et al. Hepatocytes direct the formation of a pro-metastatic niche in the liver. *Nature* **567**, 249–252 (2019).
52. Zhu, Y. et al. Tissue-resident macrophages in pancreatic ductal adenocarcinoma originate from embryonic hematopoiesis and promote tumor progression. *Immunity* **47**, 323–338 (2017).
53. Peng, H. et al. Liver-resident NK cells confer adaptive immunity in skin-contact inflammation. *J. Clin. Invest.* **123**, 1444–1456 (2013).
54. Hafemeister, C. & Satija, R. Normalization and variance stabilization of single-cell RNA-seq data using regularized negative binomial regression. *Genome Biol.* **20**, 296 2019).
55. Wu, T. et al. clusterProfiler 4.0: A universal enrichment tool for interpreting omics data. *Innovation (Camb)* **2**, (2021).
56. Tsujikawa, T. et al. Quantitative multiplex immunohistochemistry reveals myeloid-inflamed tumor-immune complexity associated with poor prognosis. *Cell Rep.* **19**, 203–217 (2017).

Acknowledgements

Author contributions

J.M.B. and D.G.D. conceived of and designed experiments, and wrote the manuscript with input from all authors. J.M.B., C.Z., L.I.K., A.A.L., N.C.B., B.L.K., S.J.B., Y.Z., L.Y., J.P.L. and D.G.D. performed experiments and analyzed data. N.C.B., Y.Z., M.A.L., N.Z., K.W.K., R.C.F., W.M.Y., L.D., J.C.M. and G.J.R. provided key resources, expertise, input and tissues.

Competing interests

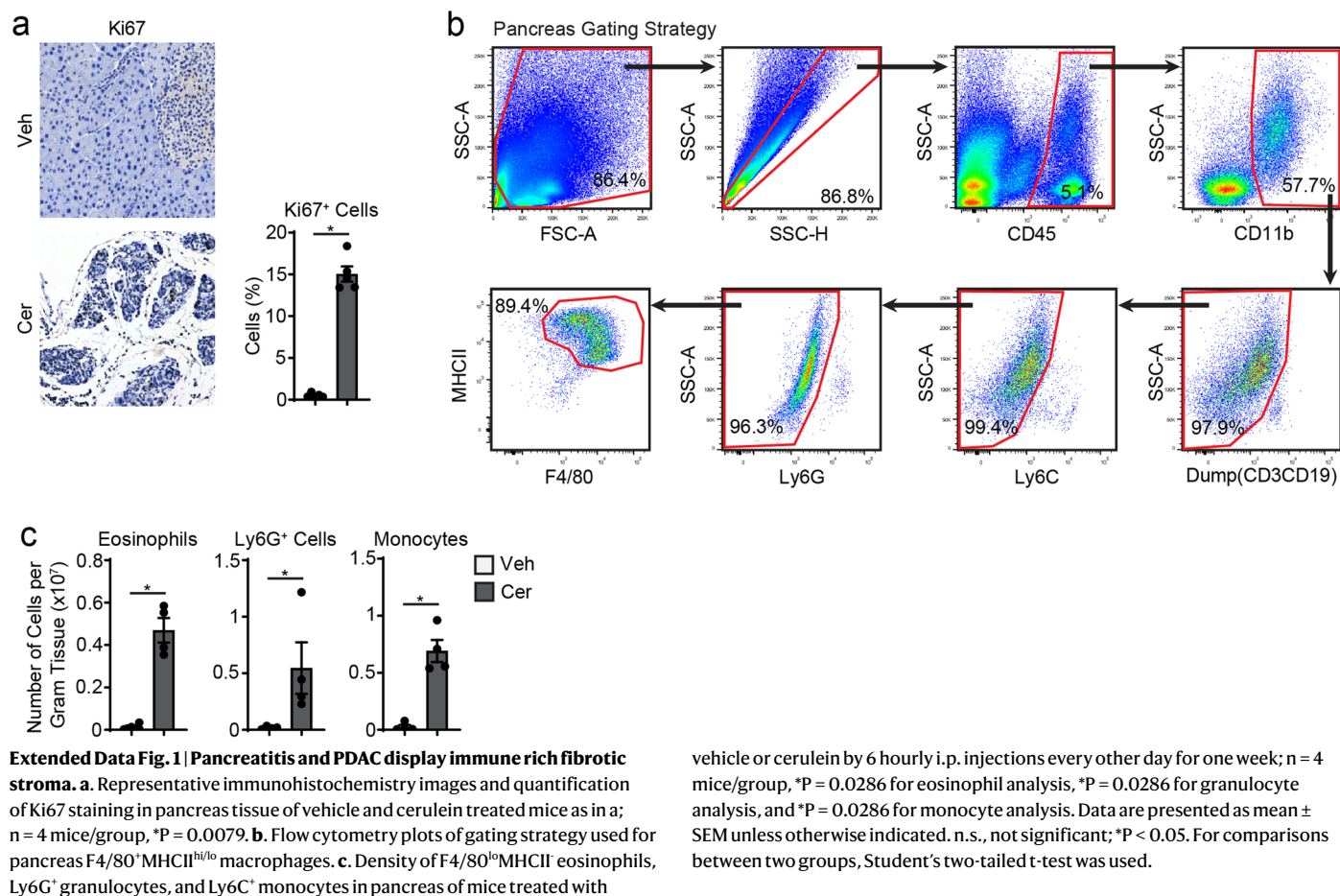The authors declare no competing interests.

Additional information
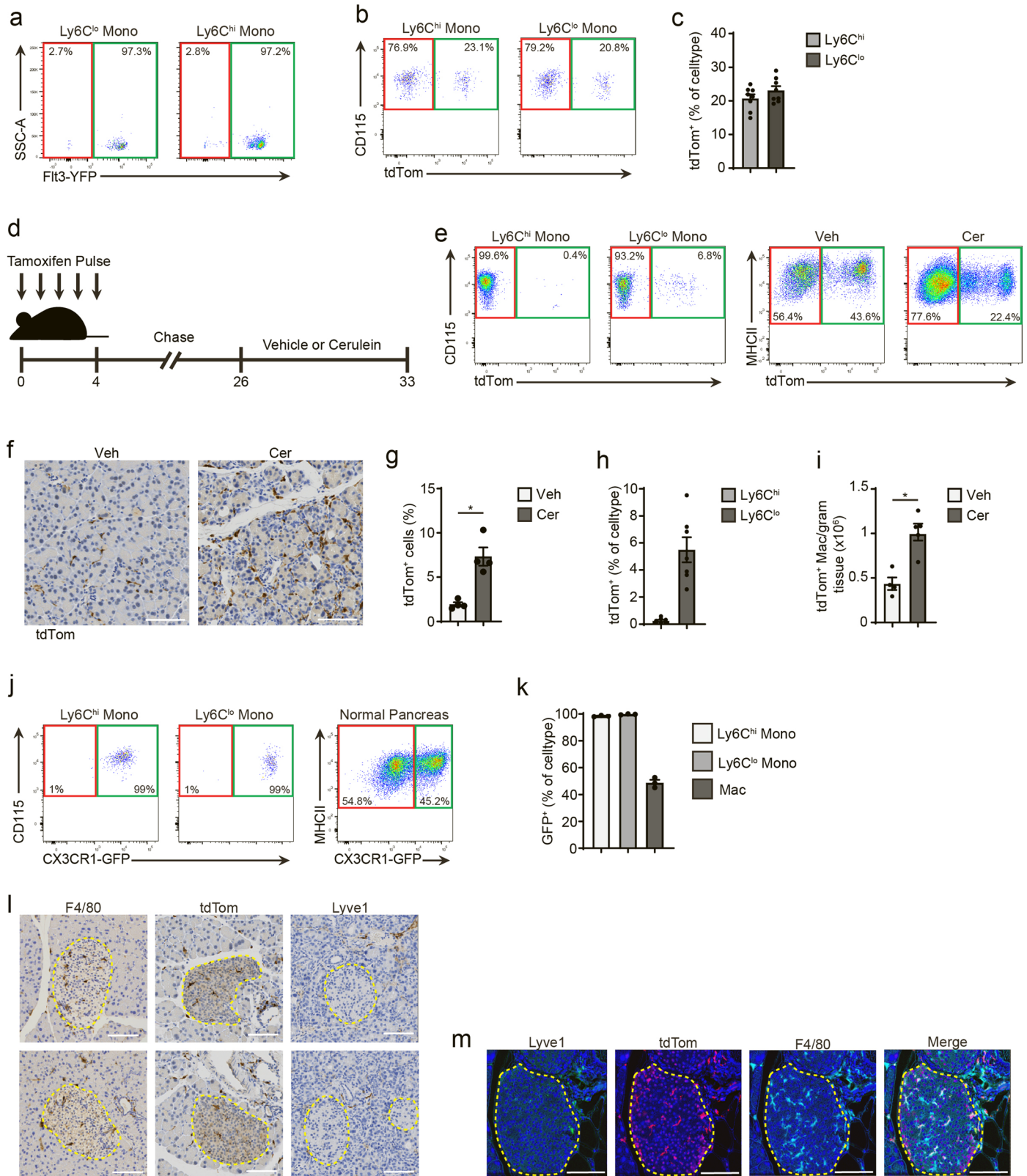
Extended data is available for this paper at https://doi.org/10.1038/s41590-023-01579-x.

Supplementary information The online version contains supplementary material available at https://doi.org/10.1038/s41590-023-01579-x.

Correspondence and requests for materials should be addressed to David G. DeNardo.

Peer review information *Nature Immunology* thanks the anonymous reviewers for their contribution to the peer review of this work. Primary Handling Editor: Ioana Visan, in collaboration with the *Nature Immunology* team. Peer reviewer reports are available.

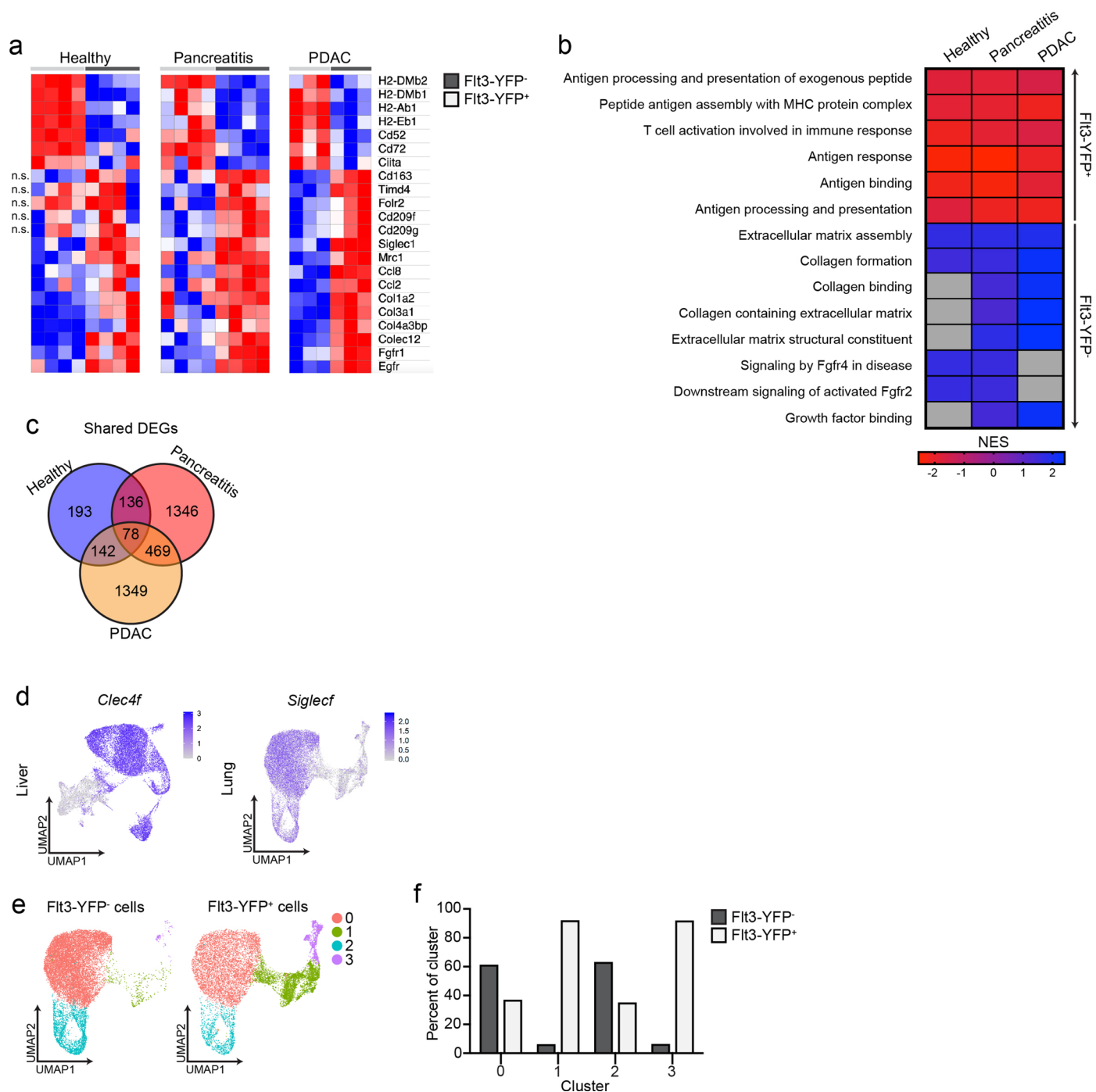**Reprints and permissions information** is available at www.nature.com/reprints.

Extended Data Fig. 1 | Pancreatitis and PDAC display immune rich fibrotic stroma. a. Representative immunohistochemistry images and quantification of Ki67 staining in pancreas tissue of vehicle and cerulein treated mice as in a; n = 4 mice/group, *P = 0.0079. **b**. Flow cytometry plots of gating strategy used for pancreas F4/80$^+$MHCII$^{hi/lo}$ macrophages. **c**. Density of F4/80^{lo}MHCII$^-$ eosinophils, Ly6G$^+$ granulocytes, and Ly6C$^+$ monocytes in pancreas of mice treated with vehicle or cerulein by 6 hourly i.p. injections every other day for one week; n = 4 mice/group, *P = 0.0286 for eosinophil analysis, *P = 0.0286 for granulocyte analysis, and *P = 0.0286 for monocyte analysis. Data are presented as mean ± SEM unless otherwise indicated. n.s., not significant; *P < 0.05. For comparisons between two groups, Student's two-tailed t-test was used.

Extended Data Fig. 2 | See next page for caption.

Extended Data Fig. 2 | Cerulein treatment increases tissue-resident macrophages. a. Flow cytometry of Flt3-YFP$^{+/-}$ cells pre-gated on blood Ly6C$^{lo/hi}$ monocytes. **b**. Flow cytometry of CSF1R-tdTom mice given tamoxifen by oral-gavage for five consecutive days, then tamoxifen was stopped for 10 weeks, pre-gated on Ly6C$^{hi/lo}$ blood monocytes. **c**. Quantification of tdTomato$^+$ Ly6C$^{hi/lo}$ blood monocytes after treatment as in b, displayed as percentage of each cell type; n = 8mice/group. **d**. Schematic of tamoxifen treatment in CX3CR1-CreERT2;LSL-tdTomato mice (hereafter CX3CR1-tdTom mice). **e**. Flow cytometry of tdTomato$^{-/+}$ cells in CX3CR1-tdTom mice treated as in d followed by vehicle or cerulein by 6 hourly i.p. injections every other day for one week, pre-gated on Ly6C$^{hi/lo}$ blood monocytes, and F4/80$^+$MHCII$^{hi/lo}$ pancreas macrophages. **f**. Representative images of IHC staining of tdTomato in pancreas tissue of CX3CR1-tdTom mice treated as in e, scale bars, 100 μM. **g**. Quantification of tdTomato$^+$ cells from pancreas tissue of CX3CR1-tdTom mice treated as in e, displayed as percentage of cells; n = 4mice/group, *P = 0.0286. **h**. Quantification of tdTomato$^+$ blood Ly6C$^{hi/lo}$ monocytes from CX3CR1-tdTom mice treated as in e, displayed as percentage of each cell type; n = 7mice/group. **i**. Density of tdTomato$^+$ pancreas

F4/80$^+$MHCII$^{hi/lo}$ macrophages from CX3CR1-tdTom mice treated as in e; vehicle, n = 4 mice; cerulein, n = 5 mice, *P = 0.0159. **j**. Flow cytometry of GFP in CX3CR1-GFP mice, pre-gated on Ly6C$^{hi/lo}$ blood monocytes, and pancreas F4/80$^+$MHCII$^{hi/lo}$ macrophages. **k**. Quantification of GFP$^+$ blood Ly6C$^{hi/lo}$ monocytes and pancreas F4/80$^+$MHCII$^{hi/lo}$ pancreas macrophages from CX3CR1-GFP mice, displayed as percentage of each cell type; n = 3mice/group. **l**. Representative images of IHC staining of pancreas tissue from CX3CR1-tdTom mice treated as in e and stained for F4/80, tdTomato, and LYVE1, islets of Langerhans outlined in yellow, scale bars, 100 μM, staining was repeated for 8 mice. **m**. Representative images of multiplex-IHC (mIHC) staining of pancreas tissue from CSF1R-tdTom mice treated with tamoxifen as in b, followed by cerulein treatment as in e, and stained for LYVE1, tdTomato, and F4/80, islet of Langerhans outlined in yellow dash, scale bars, 100 μM, staining was repeated for 4 vehicle- and 4 cerulein-treated mice. Data are presented as mean ± SEM unless otherwise indicated. n.s., not significant; *p < 0.05. For comparisons between two groups, Student's two-tailed t-test was used.
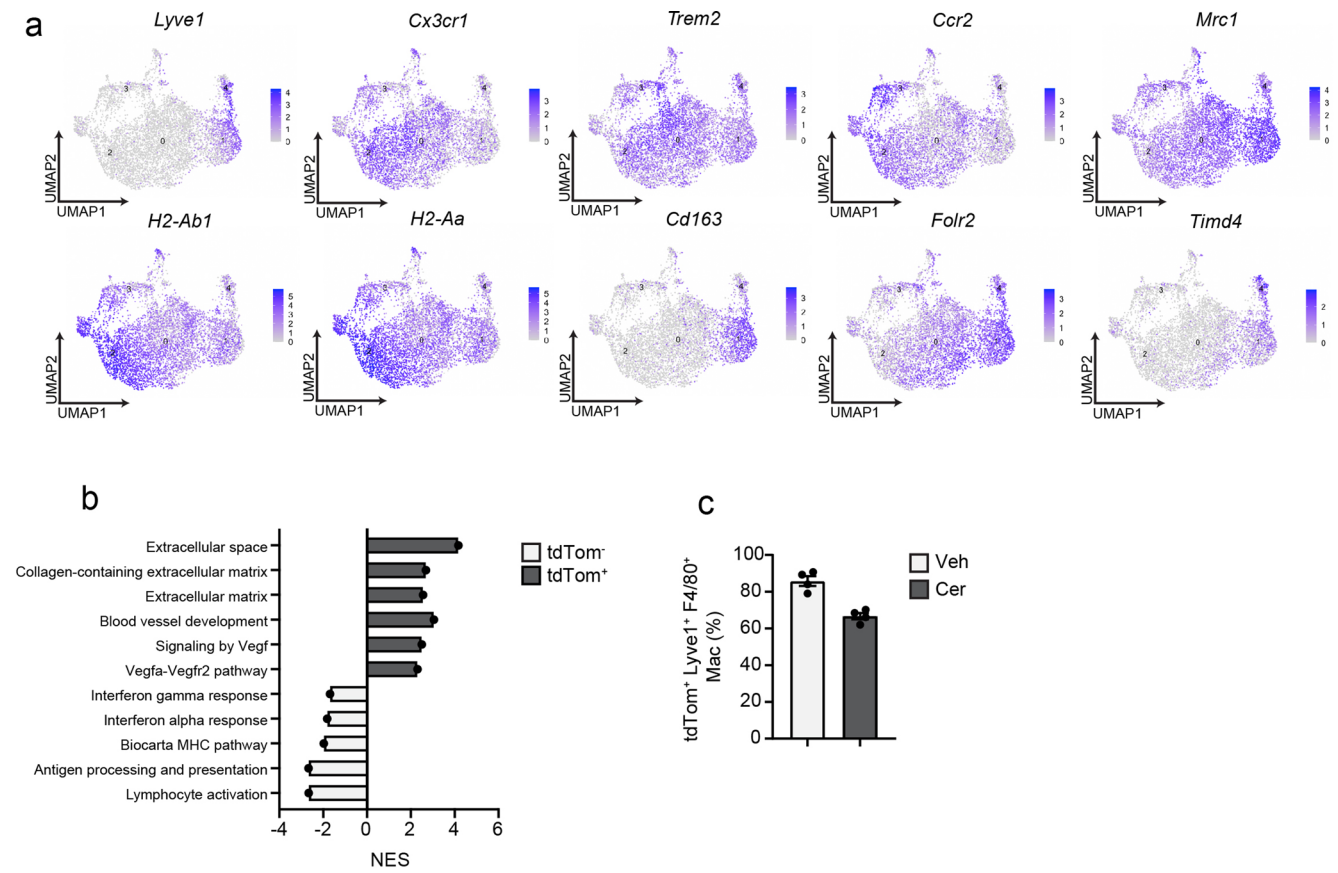
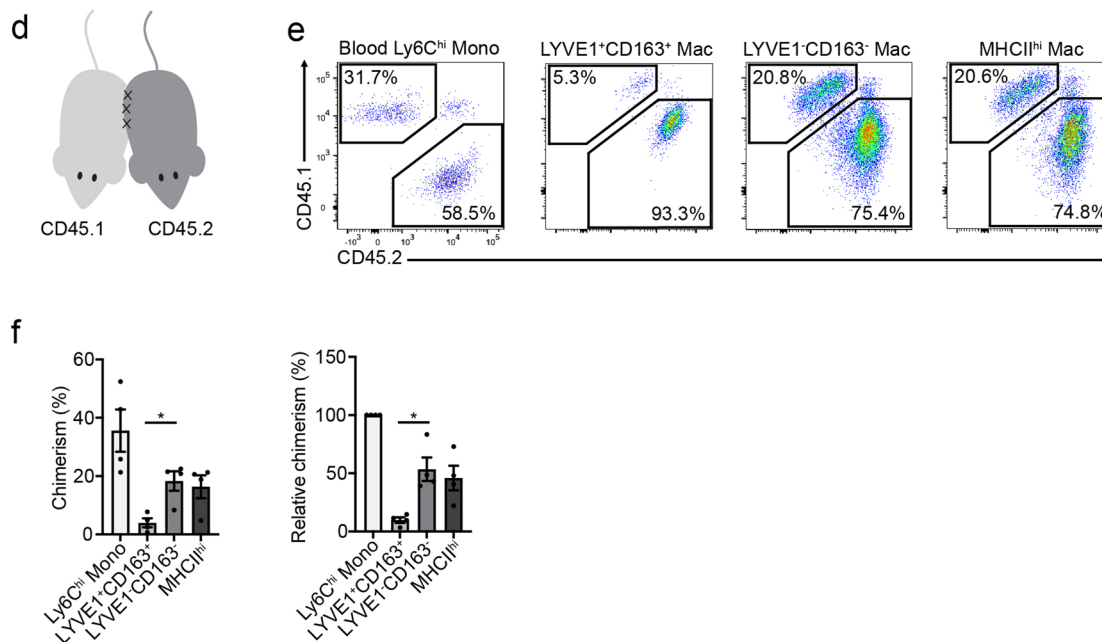Extended Data Fig. 4 | See next page for caption.

Extended Data Fig. 4 | Pancreas TRMs have distinct transcriptional phenotypes. a. UMAP plot of scRNAseq analysis of F4/80$^+$MHCII$^{hi/lo}$ macrophages sorted from pancreas of Flt3-YFP mice treated with vehicle by 6 hourly i.p. injections every other day for one week. **b**. Quantification of Flt3-YFP$^+$ and Flt3-YFP$^-$ pancreas macrophages by cluster from UMAP in a, displayed as percentage of each cluster. **c**. UMAP plot of scRNAseq analysis of F4/80$^+$MHCII$^{hi/lo}$ macrophages sorted from pancreas of Flt3-YFP mice orthotopically implanted with the KP1 pancreatic cancer cell line. **d**. Quantification of Flt3-YFP$^+$ and Flt3-YFP$^-$ pancreas macrophages by cluster from UMAP in c, displayed as percentage of each cluster. **e**. UMAP plots displaying *Timd4, Trem2, Folr2, H2-Aa, Cd74*, and *Cd14* expression in *Csf1r* and *C1qa* expressing pancreas macrophages from Flt3-YFP mice treated with cerulein by 6 hourly i.p. injections every other day for one

week. **f**. Violin plots displaying expression of *Lyve1* and *Cx3cr1* for each cluster of *Csf1r* and *C1qa* expressing pancreas macrophages from Flt3-YFP mice treated with cerulein as in a. **g**. UMAP plots displaying *Lyve1, Cx3cr1, and Ccr2* expression in F4/80$^+$MHCII$^{hi/lo}$ macrophages sorted from pancreas of Flt3-YFP mice treated as in a. **h**. UMAP plots displaying *Lyve1, Cx3cr1, and Ccr2* expression in F4/80$^+$MHCII$^{hi/lo}$ macrophages sorted from pancreas of Flt3-YFP mice implanted with tumors as in c. **i**. Bar graph of normalized enrichment score (NES) values of gene sets upregulated in Flt3-YFP$^+$ or Flt3-YFP$^-$ pancreas macrophages within pancreatitis cluster 0 (from Fig. 3c). Data are presented as mean ± SEM unless otherwise indicated. n.s., not significant; *p < 0.05. For comparisons between two groups, Student's two-tailed t-test was used, except i where FDR was used.

Parabiosis Monocyte Tracing

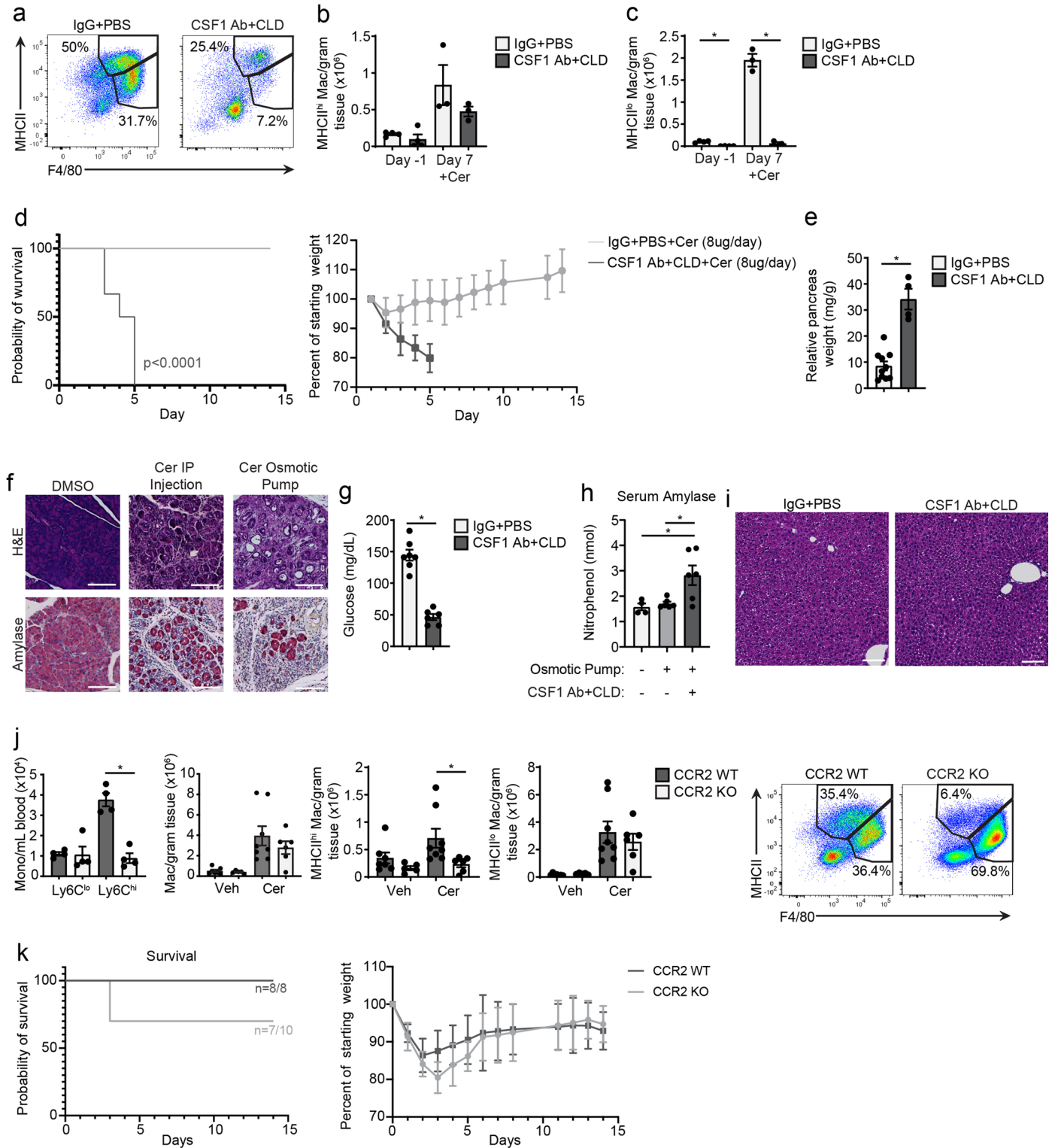**Extended Data Fig. 5 | See next page for caption.**

Extended Data Fig. 5 | Pancreas TRMs have distinct transcriptional phenotypes. a. UMAP plots displaying *Lyve1, Cx3cr1, Trem2, Ccr2, Mrc1, H2-Ab1, H2-Aa, Cd163, Folr2*, and *Timd4* expression in *Csf1r* and *C1qa* expressing pancreas macrophages from CSF1R- tdTom mice given tamoxifen by oral gavage for five consecutive days, then tamoxifen was stopped for 10 weeks, then cerulein (cer) was given by 6 hourly i.p. injections every other day for one week. **b**. Bar graph of NES values of gene sets upregulated in tdTomato⁺ or tdTomato⁻ cells from CSF1R-tdTom mice treated as in a. **c**. Quantification of LYVE1⁺F4/80⁺tdTomato⁺ pancreas macrophages from CSF1R-tdTom mice treated with tamoxifen as in a, followed by vehicle (veh) or cerulein (cer) treatment as in a, displayed as percentage of LYVE1⁺F4/80⁺ macrophages; n = 4 mice/group. **d**. Schematic of surgical joining of

parabiotic pairs of CD45.1⁺ and CD45.2⁺ C57BL/6 mice. **e**. Flow cytometry staining of CD45.1 and CD45.2 in parabiotic pairs of mice, following 6 weeks of surgical joining, pre-gated on blood Ly6C⁺ monocytes or F4/80⁺MHCII^hi/lo pancreas macrophages. **f**. Quantification of percent chimerism (left) and chimerism normalized to blood Ly6C^hi monocyte chimerism (relative chimerism, right) for blood Ly6Chi monocytes, LYVE1⁺CD163⁺ pancreas macrophages, LYVE1⁺CD163⁺ pancreas macrophages, and MHCII^hi pancreas macrophages; n = 4 mice/group, *P = 0.0286 for chimerism analysis and *P = 0.0286 for relative chimerism analysis. Data are presented as mean ± SEM unless otherwise indicated. n.s., not significant; *p < 0.05. For comparisons between two groups, Student's two-tailed t-test was used, except b where FDR was used.
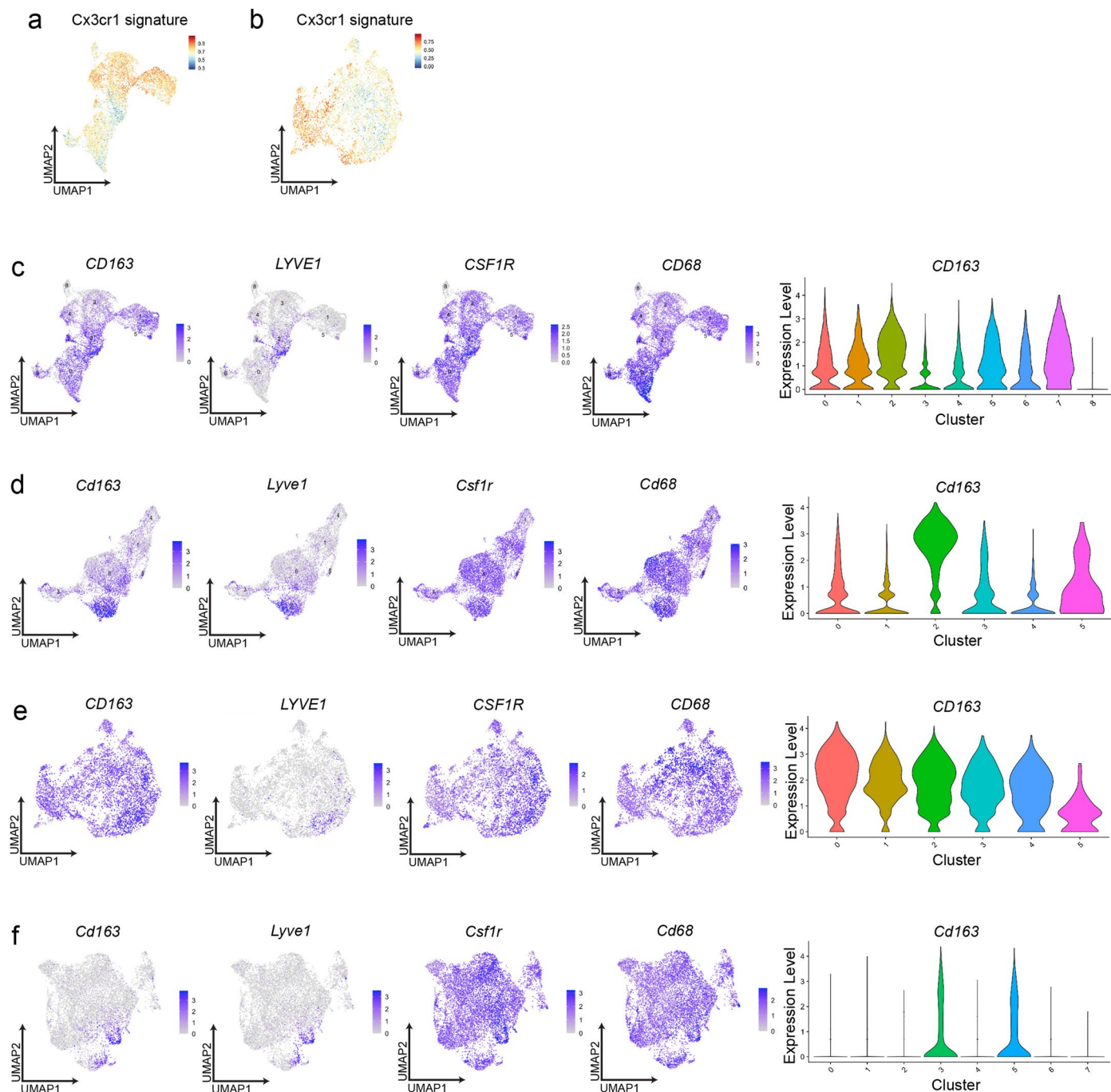
Extended Data Fig. 6 | Human LYVE1+ TRMs display similar phenotype and localization. a. UMAP plot displaying mouse LYVE1^lo pancreas macrophage scRNA-seq signature using top 100 DEGs from mouse LYVE1^lo macrophages mapped into human chronic pancreatitis data set[8]. **b.** UMAP plot displaying mouse LYVE1^lo pancreas macrophage scRNA-seq signature using top 100 DEGs from mouse LYVE1^lo macrophages mapped into published human PDAC data set[6]. **c.** UMAP plots displaying *CD163, LYVE1, CSF1R*, and *CD68* expression in human healthy and chronic pancreatitis samples from a, and violin plot showing *CD163* gene expression across human pancreatitis macrophage clusters. **d.** UMAP plots displaying *Cd163, Lyve1, Csf1r*, and *Cd68* expression in scRNA-seq of F4/80^+MHCII^hi/lo macrophages sorted from the pancreas of Flt3-YFP mice

treated with cerulein by 6 hourly i.p. injections every other day for one week, and violin plot showing *Cd163* gene expression across same dataset of mouse pancreas macrophage clusters. **e.** UMAP plots displaying *CD163, LYVE1, CSF1R*, and *CD68* expression in macrophages from human PDAC data set as in b, and violin plot showing *CD163* gene expression across human PDAC macrophage clusters. **f.** UMAP plots displaying *Cd163, Lyve1, Csf1r*, and *Cd68* expression in mouse F4/80^+MHCII^hi/lo macrophages sorted from pancreas of Flt3-YFP mice orthotopically implanted with the KP1 pancreatic cancer cell line, and violin plot showing *Cd163* gene expression across same dataset of mouse PDAC macrophage clusters.
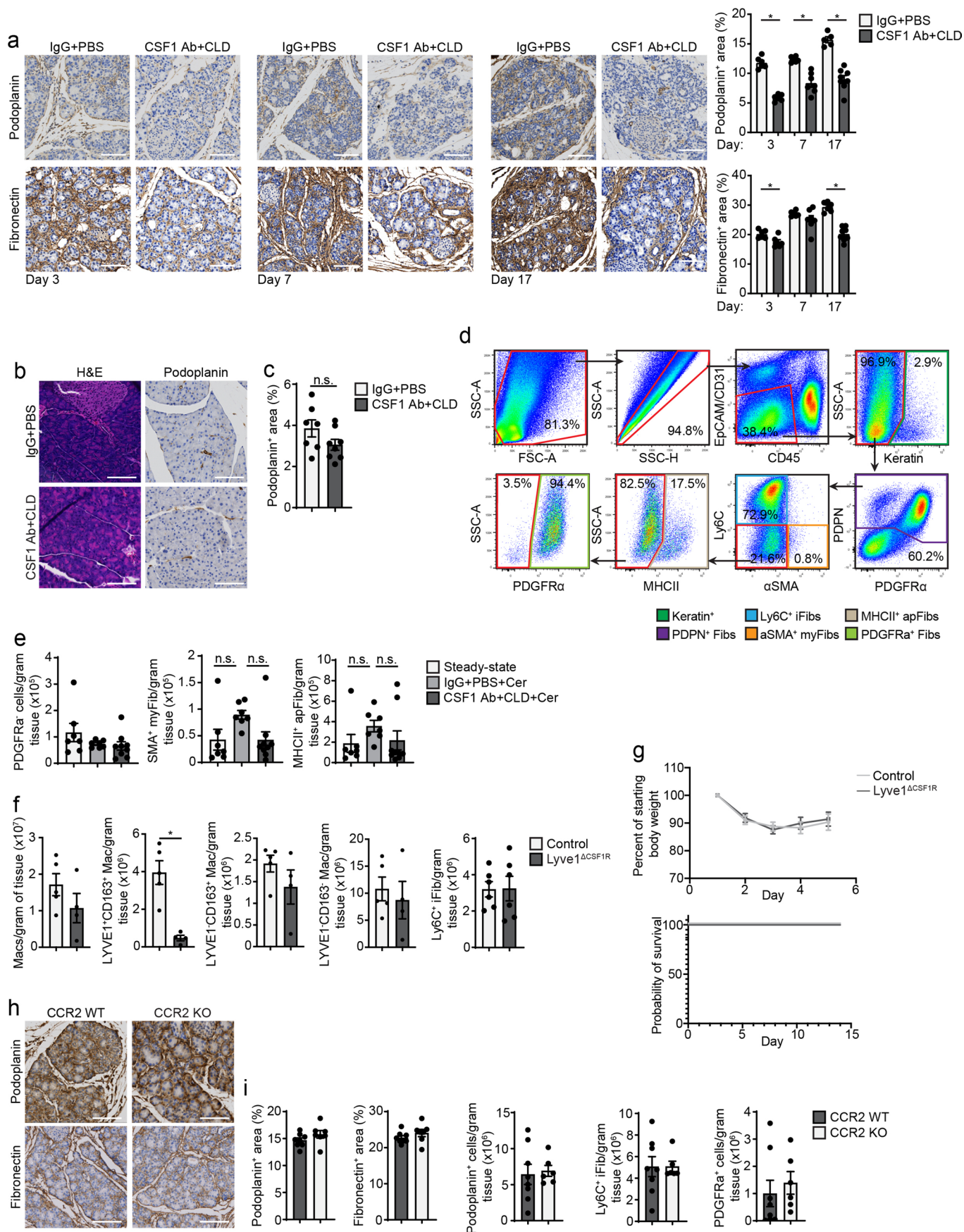
Extended Data Fig. 7 | See next page for caption.

Extended Data Fig. 7 | TRMs maintain tissue integrity during pancreatitis.
a. Flow cytometry of pancreas F4/80$^+$MHCII$^{hi/lo}$ macrophages after treatment with CSF1Ab+CLD or IgG+PBS, then a 10-day recovery period (day -1), then cerulein (cer) treatment by 6 hourly i.p. injections every other day for one week (day 7). **b**. Density of MHCII^{hi} pancreas macrophages from mice treated as in a; day -1, n = 4mice/group; day 7, n = 3mice/group. **c**. Density of MHCII^{lo} pancreas macrophages from mice treated as in a; day -1, n = 4mice/group; day 7, n = 3mice/group, left to right *P = 0.0002 and *P = 0.0002. **d**. Kaplan-Meier survival curve and body weight measurement of C57BL/6 mice treated with IgG+PBS or CSF1Ab+CLD as in a, followed by cerulein-loaded osmotic pump (10 μg/day cerulein) implantation; IgG+PBS, n = 10mice; CSF1 Ab+CLD, n = 6mice, *P < 0.0001 in survival analysis. **e**. Relative pancreas weight in C57BL/6 mice treated as in d; IgG+PBS, n = 10mice, CSF1Ab+CLD, n = 4mice, *P < 0.0020. **f**. IHC images of H&E and amylase stain in pancreas from mice implanted with DMSO-loaded osmotic pump, cerulein treatment as in a, or cerulein-loaded osmotic pump, scale bars, 100 μM. **g**. Blood glucose concentration at humane survival endpoint in mice treated as in d; IgG+PBS, n = 7mice; CSF1Ab+CLD, n = 6mice, *P = 0.0012.
h. Serum amylase level in mice treated as in f; left to right n = 4mice, n = 6mice, and n = 6mice, and *P = 0.0381 and *P = 0.0390. **i**. H&E-stained liver from mice treated as in f, scale bars, 100 μM. **j**. Blood Ly6C^{lo} and Ly6C^{hi} monocytes, and pancreas F4/80$^+$, F4/80$^+$MHCII^{hi}, and F4/80$^+$MHCII^{lo} macrophages, and flow cytometry of F4/80$^+$MHCII$^{hi/lo}$ pancreas macrophages in CCR2-WT and CCR2-KO mice treated with cerulein by i.p. injection as in a; n = 4 mice/group and *P = 0.0286 in blood Ly6C^{lo} and Ly6C^{hi} analysis, n = 7 mice in veh CCR2-WT group, n = 5 mice in veh CCR2-KO group, n = 8 mice in cer CCR2-WT group, and n = 6 in cer CCR2-KO group in F4/80$^+$, F4/80$^+$MHCII^{hi}, and F4/80$^+$MHCII^{lo} analyses, and *P = 0.0047 in F4/80$^+$MHCII^{hi} macrophage analysis. **k**. Kaplan-Meier survival curve and body weight measurement of CCR2-WT and CCR2-KO mice implanted with cerulein-loaded osmotic pumps, as in d; n = 8 mice in CCR2-WT group, n = 10 mice in CCR2-KO group. Data are presented as mean ± SEM unless otherwise indicated. n.s., not significant; *p < 0.05. For comparisons between two groups, Student's two-tailed t-test was used.
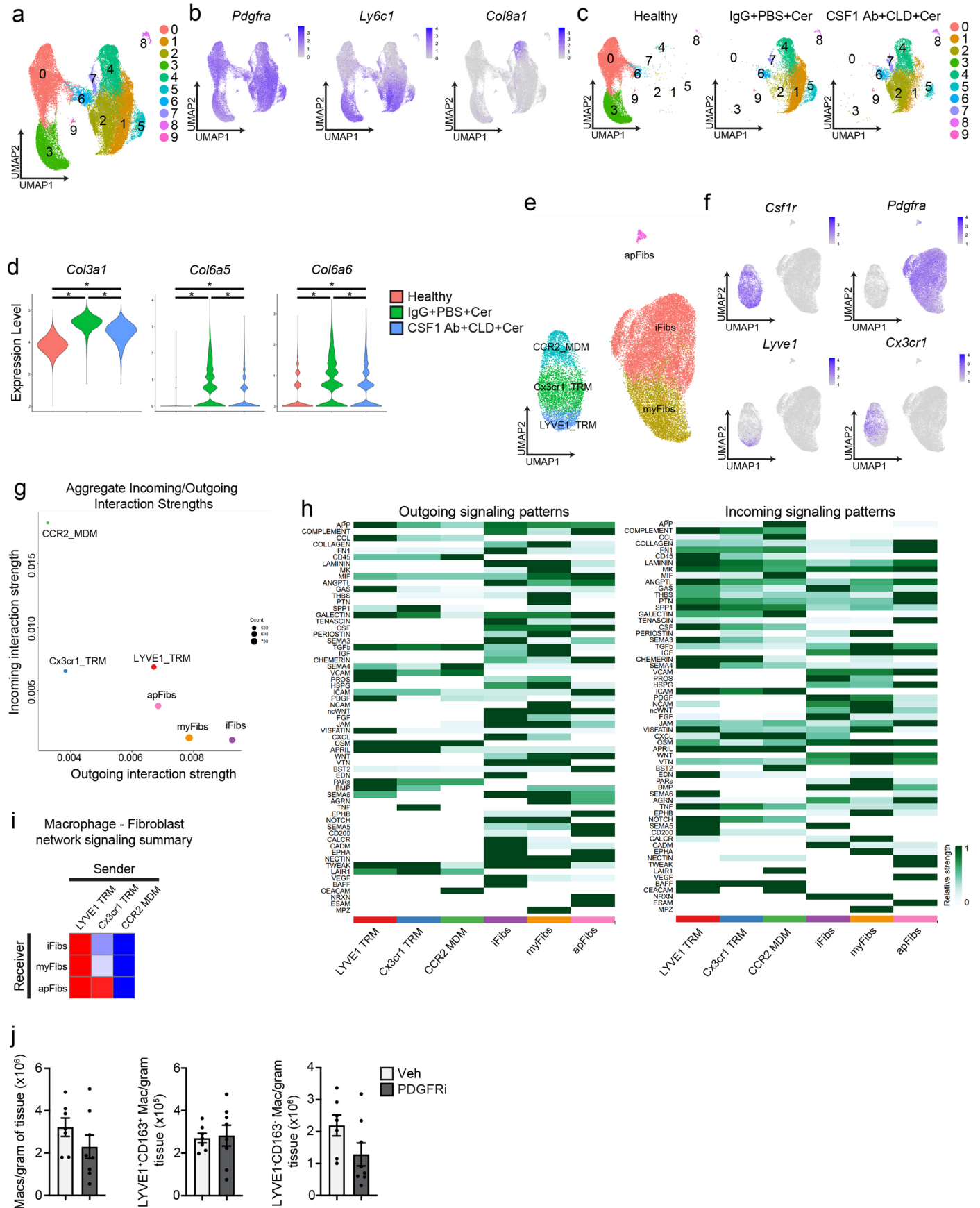
Extended Data Fig. 8 | See next page for caption.

Extended Data Fig. 8 | Depletion of TRMs attenuates fibrotic responses.
a. IHC staining and quantification for podoplanin and fibronectin on pancreas tissue from mice treated with CSF1Ab+CLD or IgG+PBS, then a 10-day recovery period, then cerulein (cer) treatment by 6 hourly i.p. injections every other day for 3, 7, or 17 days, scale bars, 100 μM, IgG+PBS, CSF1Ab+CLD day 3, and IgG+PBS day 7, n = 6mice; CSF1Ab+CLD day 7, n = 7mice; IgG+PBS day 17, n = 5mice; CSF1Ab+CLD day 17, n = 8mice; podoplanin left to right, *P = 0.0022, *P = 0.0012, and *P = 0.0016; fibronectin left to right, *P = 0.0130 and *P = 0.0007. **b**. H&E and podoplanin stained pancreas tissue from mice treated as in a, with no cerulein treatment, scale bars, 100 μM. **c**. Podoplanin IHC quantification on pancreas tissue of mice treated as in b; IgG+PBS, n = 7mice; CSF1Ab+CLD, n = 8mice. **d**. Flow cytometry gating for pancreas fibroblast subsets. **e**. Density of pancreas PDGFRα$^-$, α-SMA$^+$, and MHCII$^+$ fibroblasts from mice treated with IgG+PBS followed by vehicle (steady-state), IgG+PBS followed by cerulein (IgG+PBS+Cer), and CSF1Ab+CLD followed by cerulein (CSF1 AB+CLD+Cer) as in a; steady-state and IgG+PBS+Cer, n = 7mice, and CSF1Ab+CLD+Cer, n = 9mice. **f**. Density

of pancreas F4/80$^+$MHCII$^{hi/lo}$, LYVE1$^+$CD163$^+$, LYVE1$^-$CD163$^+$, LYVE1$^-$CD163$^-$ macrophages, and Ly6C$^+$ iFibs in Lyve1-Cre$^-$ littermate controls (control), or Lyve1^{ΔCSF1R} mice treated with cerulein by i.p. injections every other day for one week; control, n = 5mice; Lyve1^{ΔCSF1R}, n = 4mice; LYVE1$^+$CD163$^+$, *P = 0.0159, and Ly6C$^+$ iFib, n = 6mice/group. **g**. Mouse body weight measurement and Kaplan-Meier survival curve following implantation of osmotic pump for delivery of 10 μg/day cerulein in control or Lyve1^{ΔCSF1R} mice; n = 9 mice in control and n = 8 mice in Lyve1^{ΔCSF1R} group. **h**. Podoplanin and fibronectin IHC staining on pancreas tissue of CCR2-WT and CCR2-KO mice treated with cerulein as in f; scale bars, 100 μM. **i**. Quantification of podoplanin and fibronectin IHC stains and density of podoplanin$^+$ fibroblasts, Ly6C$^+$ iFibs, and PDGFRα$^+$ fibroblasts in pancreas tissue of CCR2-WT and CCR2-KO mice treated with cerulein as in f; CCR2-WT, n = 8mice; CCR2-KO, n = 7mice for podoplanin and fibronectin IHC analyses, and CCR2-WT, n = 8mice; CCR2-KO, n = 6mice for fibroblast flow cytometry analyses. Data are presented as mean ± SEM unless otherwise indicated. n.s., not significant; *p < 0.05. For comparisons between two groups, Student's two-tailed t-test was used.
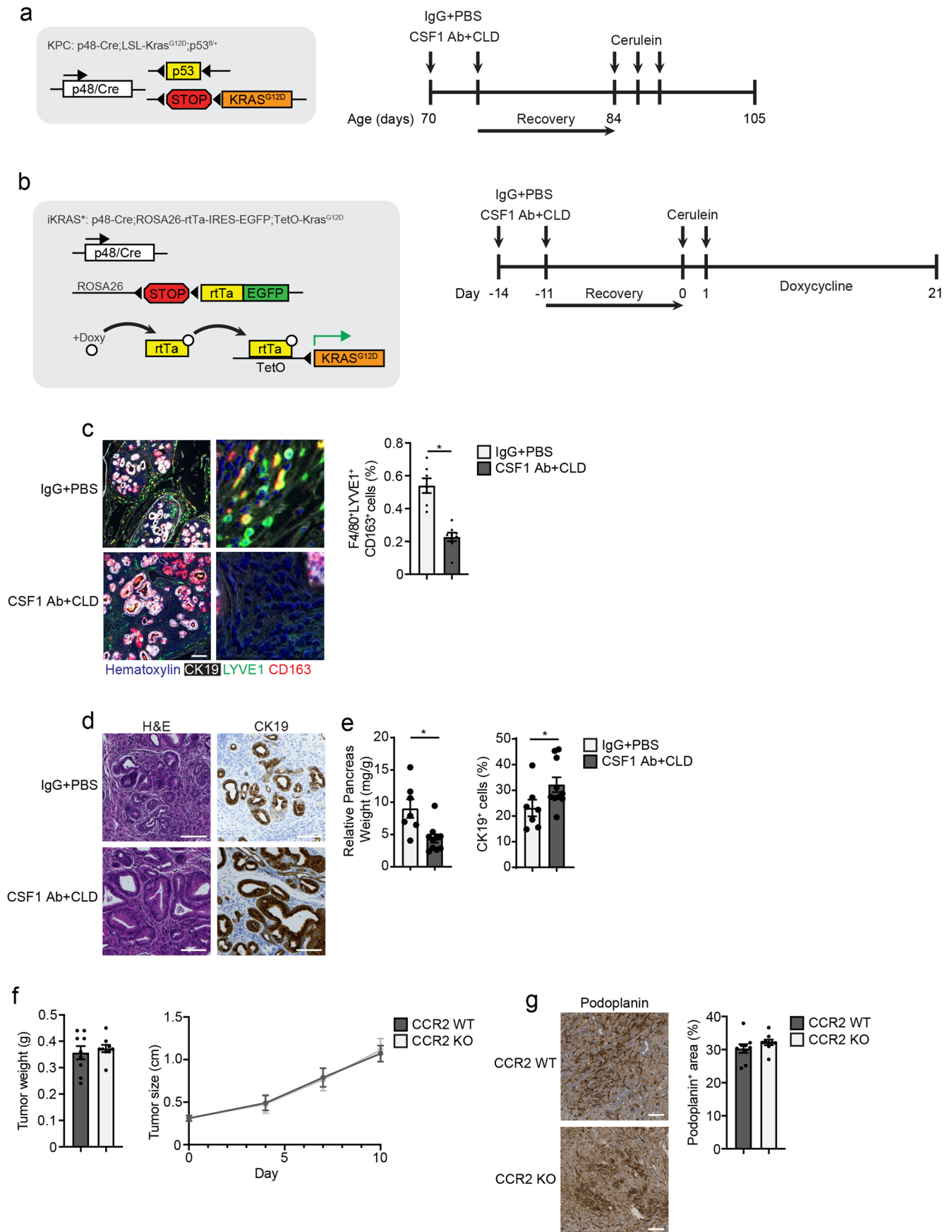
Extended Data Fig. 9 | See next page for caption.

Extended Data Fig. 9 | TRMs shape the tissue-protective fibrotic response. a. UMAP plot of scRNA-seq analysis of PDPN⁺ pancreas fibroblasts sorted from mice treated with IgG+PBS followed by vehicle (healthy), IgG+PBS followed by cerulein (IgG+PBS+Cer), and CSF1 Ab+CLD followed by cerulein (CSF1 Ab+CLD+Cer). **b**. UMAP plots displaying expression of *Pdgfra, Ly6c1*, and *Col8a1* in PDPN⁺ fibroblasts from a. **c**. UMAP plot of pancreas PDPN⁺ fibroblasts separated by healthy, IgG+PBS+Cer, or CSF1 Ab+CLD+Cer samples as in a. **d**. Violin plot of *Col3a1, Col6a5*, and *Col6a6* expression across samples (healthy, IgG+PBS+Cer, or CSF1 Ab+CLD+Cer); for all comparisons *P < 0.0001. **e**. UMAP plot of scRNA-seq analysis combining macrophages from Flt3-YFP mice treated with cerulein and fibroblasts from IgG+PBS+Cer and CSF1 Ab+CLD+Cer treated mice. **f**. UMAP plots displaying *Csf1r, Pdgfra, Lyve1*, and *Cx3cr1* expression in combined macrophage and fibroblast scRNA-seq analysis from e. **g**. Dot plot showing aggregate score of all incoming (receptor) and outgoing (ligand) interactions summarized for each macrophage and fibroblast cluster from e, as measured by CellChat[9]. **h**. Heatmap displaying relative strength of network centrality measures for outgoing (ligands, left heatmap) and incoming (receptors, right heatmap) signaling patterns of each intercellular signaling pathway. **i**. Heatmap displaying aggregate score across all differentially enriched receptor (receiver) or ligand (sender) pathways between macrophage and fibroblast clusters from e. **j**. Density of pancreas F4/80⁺MHCII^hi/lo, LYVE1⁺CD163⁺, and LYVE1⁻CD163⁻ macrophages from mice treated with vehicle (veh) or PDGFRi once per day by i.p. injection along with cerulein treatment by 6 hourly i.p. injections every other day for one week; n = 7 mice in vehicle and n = 8 mice in PDGFRi groups. Data are presented as mean ± SEM unless otherwise indicated. n.s., not significant; *p < 0.05. For comparisons between two groups, Student's two-tailed t-test was used, except for d where Bonferroni correction was used.

Extended Data Fig. 10 | See next page for caption.

Extended Data Fig. 10 | TRMs drive fibrosis and pancreatitis-accelerated PDAC progression. a. Genetic loci for p48-Cre;LSL-KRAS^{G12D};p53$^{fl/+}$ (KPC) model and treatment scheme for IgG+PBS and CSF1 Ab+CLD followed by cerulein by 6 hourly i.p injections every other day for 5 days. **b**. Genetic loci for p48-Cre;ROSA26-rtTa-IRES-EGFP;TetO-KRAS^{G12D} (iKRAS*) model and treatment scheme for IgG+PBS and CSF1 Ab+CLD followed by cerulein by 6 hourly i.p injections on two consecutive days, followed by doxycycline administration in drinking water. **c**. Representative mIHC images of pancreas tissue from iKRAS* mice treated with IgG+PBS or CSF1 Ab+CLD as in b, stained for hematoxylin, CK19, F4/80, LYVE1, and CD163 (scale bars are 100 μM), and quantification of F4/80^{+}LYVE1^{+}CD163^{+} macrophages, displayed as the percentage of cells; n = 7 mice in IgG+PBS group, n = 8 mice in CSF1 Ab+CLD group, and *P = 0.0003. **d**. Representative images of pancreas tissue stained for H&E and CK19 from iKRAS* mice treated with IgG+PBS or CSF1 Ab+CLD as in b, scale bars are 100 μM. **e**. Quantification of relative pancreas weight and CK19^{+} cells displayed as percentage of total cells from iKRAS* mice treated with IgG+PBS or CSF1 Ab+CLD as in b; n = 7 mice in IgG+PBS group, n = 10 mice in CSF1 Ab+CLD group, *P = 0.0097 in relative pancreas weight analysis, and *P = 0.0250 in CK19 analysis. **f**. Tumor weight and size measurements of CCR2-WT and CCR2-KO mice orthotopically implanted with the KP2 pancreatic cancer cell line; n = 9 mice/group. **g**. Representative images and quantification of pancreas tissue from CCR2-WT and CCR2-KO mice orthotopically implanted with the KP2 pancreatic cancer cell line stained for podoplanin, scale bars are 100 μM; n = 9 mice/group. Data are presented as mean ± SEM unless otherwise indicated. n.s., not significant; *p < 0.05. For comparisons between two groups, Student's two-tailed t-test was used.

nature portfolio

Corresponding author(s): David DeNardo

Last updated by author(s): Jul 7, 2023

Reporting Summary

Nature Portfolio wishes to improve the reproducibility of the work that we publish. This form provides structure for consistency and transparency in reporting. For further information on Nature Portfolio policies, see our Editorial Policies and the Editorial Policy Checklist.

Statistics

For all statistical analyses, confirm that the following items are present in the figure legend, table legend, main text, or Methods section.

n/a	Confirmed	
☐	☒	The exact sample size (*n*) for each experimental group/condition, given as a discrete number and unit of measurement
☐	☒	A statement on whether measurements were taken from distinct samples or whether the same sample was measured repeatedly
☐	☒	The statistical test(s) used AND whether they are one- or two-sided *Only common tests should be described solely by name; describe more complex techniques in the Methods section.*
☒	☐	A description of all covariates tested
☐	☒	A description of any assumptions or corrections, such as tests of normality and adjustment for multiple comparisons
☐	☒	A full description of the statistical parameters including central tendency (e.g. means) or other basic estimates (e.g. regression coefficient) AND variation (e.g. standard deviation) or associated estimates of uncertainty (e.g. confidence intervals)
☐	☒	For null hypothesis testing, the test statistic (e.g. *F*, *t*, *r*) with confidence intervals, effect sizes, degrees of freedom and *P* value noted *Give P values as exact values whenever suitable.*
☒	☐	For Bayesian analysis, information on the choice of priors and Markov chain Monte Carlo settings
☒	☐	For hierarchical and complex designs, identification of the appropriate level for tests and full reporting of outcomes
☒	☐	Estimates of effect sizes (e.g. Cohen's *d*, Pearson's *r*), indicating how they were calculated

Our web collection on statistics for biologists contains articles on many of the points above.

Software and code

Policy information about availability of computer code

Data collection	BD FACSDiva software was used for flow cytometry, and Zeiss Zen (v3.2.0) software was used to acquire images
Data analysis	HALO (Indica Labs) software was used for all image analysis. FlowJo software was used for analysis of flow cytometry experiments. Single-cell RNA-sequencing analysis was performed using R (v3.6.3) packages Seurat (https://satijalab.org/seurat/), Harmony for data integration (https://github.com/immunogenomics/harmony), and ClusterProfiler (https://github.com/YuLab-SMU/clusterProfiler) for GSEA comparisons.

For manuscripts utilizing custom algorithms or software that are central to the research but not yet described in published literature, software must be made available to editors and reviewers. We strongly encourage code deposition in a community repository (e.g. GitHub). See the Nature Portfolio guidelines for submitting code & software for further information.

Data

Policy information about availability of data

All manuscripts must include a data availability statement. This statement should provide the following information, where applicable:
- Accession codes, unique identifiers, or web links for publicly available datasets
- A description of any restrictions on data availability
- For clinical datasets or third party data, please ensure that the statement adheres to our policy

Sequencing data (bulk and single-cell RNAseq) has been made publicly available under Gene Expression Omnibus (GEO) repository accession numbers GSE196778 (scRNAseq), and GSE203005 (bulk RNAseq). All other data are available upon request to the lead contact, David G. DeNardo (ddenardo@wustl.edu).

Human research participants

Policy information about <u>studies involving human research participants and Sex and Gender in Research.</u>

Reporting on sex and gender	All human tissue samples were provided completely de-identified aside from diagnosis. No information on age, sex, or gender were available.
Population characteristics	No human research participants were used.
Recruitment	No human research participants were used.
Ethics oversight	No human research participants were used.

Note that full information on the approval of the study protocol must also be provided in the manuscript.

Field-specific reporting

Please select the one below that is the best fit for your research. If you are not sure, read the appropriate sections before making your selection.

☒ Life sciences ☐ Behavioural & social sciences ☐ Ecological, evolutionary & environmental sciences

For a reference copy of the document with all sections, see nature.com/documents/nr-reporting-summary-flat.pdf

Life sciences study design

All studies must disclose on these points even when the disclosure is negative.

Sample size	Sample size was previously computed by biostatistician for major primary endpoints prior to conducting the experiments. All in vivo flow cytometry experiments were designed with 8 mice per group to give 95.1% power at the 5% significance level. For in vivo experiments utilizing IHC and pathologic grading, studies were designed with 8 mice per group to give 92.9% or 87.5% power respectively at the 5% significance level.
Data exclusions	Across all studies we excluded two animals based on inclusion of contamination of non-pancreas tissues in samples as determined by flow cytometry.
Replication	All in vivo mouse experiments were repeated in at least two independent cohorts of mice, and in some cases different genetic backgrounds. For all in vitro experiment, experiments were replicated at least 2 independent times with 3 biologically independent samples.
Randomization	Mice were genotyped for stain-specific alleles. Mice genotyped as positive were allocated randomly into treatment groups, littermate controls that were genotyped negative were subsequently allocated randomly into control groups when appropriate.
Blinding	All mice were assigned numbers to allow researchers to be blinded to mouse genotype or treatment group when possible. During data collection by either flow cytometry, IHC analysis, or pathological grading, mice were only referred to by their number to avoid bias towards genotype or treatment group. Data were then organized according to group or treatment once data collection was complete.

Reporting for specific materials, systems and methods

We require information from authors about some types of materials, experimental systems and methods used in many studies. Here, indicate whether each material, system or method listed is relevant to your study. If you are not sure if a list item applies to your research, read the appropriate section before selecting a response.

Materials & experimental systems

n/a	Involved in the study
☐	☒ Antibodies
☐	☒ Eukaryotic cell lines
☒	☐ Palaeontology and archaeology
☐	☒ Animals and other organisms
☐	☒ Clinical data
☒	☐ Dual use research of concern

Methods

n/a	Involved in the study
☒	☐ ChIP-seq
☐	☒ Flow cytometry
☒	☐ MRI-based neuroimaging

Antibodies

Antibodies used	
	Anti-mouse B220-APC (Clone RA3-6B2) BioLegend 1:200 Cat# 103212
	Anti-mouse CD11b-Alexa700 (Clone M1/70) eBioscience 1:400 Cat# 56-0112-82
	Anti-mouse CD16/CD32 (Clone 93) eBioscience 1:200 Cat# 14-0161-82
	Anti-mouse CD19-APC (Clone eBio1D3) eBioscience 1:200 Cat# 17-0193-82
	Anti-mouse CD45-APC-eFluor780 (Clone 30-F11) eBioscience 1:400 Cat# 47-0451-82
	Anti-mouse CD45-PE-Cy7 (Clone 30-F11) eBioscience 1:400 Cat# 25-0451-82
	Anti-mouse CD115-BV605 (Clone AFS98) BioLegend 1:200 Cat# 135517
	Anti-mouse CD115-PE (Clone AFS98) eBioscience 1:200 Cat# 12-1152-82
	Anti-mouse CX3CR1-PE (Clone SA011F11) BioLegend 1:200 Cat# 149006
	Anti-mouse F4/80-PE (Clone BM8) eBioscience 1:400 Cat# 12-4801-82
	Anti-mouse F4/80-PE-Cy5 (Clone BM8) eBioscience 1:400 Cat# 15-4801-82
	Anti-mouse Ki-67-BV605 (Clone 16A8) BioLegend 1:100 Cat# 652413
	Anti-mouse Ki-67-FITC (Clone SolA15) eBioscience 1:100 Cat# 11-5698-82
	Anti-mouse Ly6C-Alexa488 (Clone HK1.4) eBioscience 1:400 Cat# 53-5932-82
	Anti-mouse Ly6C-PerCP-Cy5.5 (Clone HK1.4) eBioscience 1:400 Cat# 45-5932-82
	Anti-mouse Ly6G-APC (Clone 1A8) BioLegend 1:400 Cat# 127614
	Anti-mouse Ly6G-PE (Clone 1A8) eBioscience 1:400 Cat# 12-9668-82
	Anti-mouse MHCII-APC-eFluor780 (Clone M5/114.15.2) eBioscience 1:400 Cat# 47-5321-82
	Anti-mouse MHCII-eFluor450 (Clone M5/114.15.2) eBioscience 1:400 Cat# 48-5321-82
	Anti-mouse SiglecF-APC (Clone ES22-10D8) Miltenyi 1:50 Cat# 130-102-241
	Anti-mouse CD45-BUV395 (Clone 30-F11) BD Pharmingen 1:400 Cat# 564279
	Anti-mouse EPCAM-BV605 (Clone G8.8) BioLegend 1:100 Cat# 118227
	Anti-mouse CD31-BV605 (Clone 390) BioLegend 1:200 Cat# 102427
	Anti-mouse Keratin-APC (Clone C11) Invitrogen 1:50 Cat# MA1-10325
	Anti-mouse PDGFRa-PE (Clone APA5) Invitrogen 1:100 Cat# 12-1401-81
	Anti-mouse PDPN-APC-Cy7 (Clone 8.1.1) BioLegend 1:400 Cat# 127418
	Anti-mouse aSMA-AlexaFluor488 (Clone 1A4) Invitrogen 1:400 Cat# 53-9760-82
	Anti-mouse Ly6C-BV785 (Clone HK1.4) BioLegend 1:400 Cat# 128041
	Anti-mouse MHCII-BV510 (Clone M5/114.15.2) BioLegend 1:400 Cat# 107636
	Anti-mouse Amylase (Polyclonal) Millipore Sigma 1:1000 A8273
	Anti-mouse Keratin 19 (Clone TROMA-III) University of Iowa DSHB 1:500 TROMA-III
	Anti-mouse Sox9 (Polyclonal) Millipore Sigma 1:1000 ABE571
	Anti-mouse Ki-67 (Clone D3B5) Cell Signaling 1:400 12202
	Anti-mouse Fibronectin (Polyclonal) Abcam 1:2000 Ab23750
	Anti-mouse Podoplanin (Clone RTD4E10) Abcam 1:1000 Ab11936
	Anti-mouse Type 1 Collagen (Polyclonal) Southern Biotech 1:50 1310-01
	Anti-mouse F4/80 (Clone D2S9R) Cell Signaling 1:200 70076
	Anti-mouse Lyve1 (Clone Aly7, biotinylated) eBioscience 1:500 13-0443-82
	Anti-mouse CD163 (EPR19518) Abcam 1:500 Ab182422
	Anti-RFP (Polyclonal) Rockland 1:200 600-401-379
	Anti-GFP (Clone EPR14104) Abcam 1:200 Ab183734
	Anti-Keratin 17/19 (Clone D4G2) Cell Signaling 1:500 12434
	Anti-Cleaved Caspase 3 (Clone ASP175) Cell Signaling 1:200 9661S
	Anti-Mouse Alpha Smooth Muscle Actin Abcam 1:100 Ab5694
	Anti Collagen VI Abcam 1:400 Ab6588
	Anti Collagen IV Abcam 1:400 Ab6586
	Anti-Human PDPN BioLegend 1:50 916602
	Anti-Human LYVE1 (EPR21857) Abcam 1:750 Ab219556
	Anti-Human CD163 Leica Biosystems 1:200 Leica NCL-L-CD163
	Anti-Rat Rabbit Secondary Vector 1:500 AI-4001
	Anti-Rat Biotin Secondary Vector 1:500 BA-9400
	Anti-Syrian Hamster Biotin Abcam 1:500 Ab7145
Validation	All antibodies were commercially validated. Validation data is available on manufacturer website. Commercial validation involves western blot analysis for presence of single band typically.

Eukaryotic cell lines

Policy information about cell lines and Sex and Gender in Research

Cell line source(s)	
	KPC-1 (Mitchem et al., 2013) cell line was derived from a 2.2 month old female KPPC mouse (p48-Cre;LSL-KRASG12D;p53fl/fl), and grown on collagen-coated tissue culture flasks for < 12 generations.
	KPL86 cell line was derived from lung tissues of the 9-month-old female KrasLSL-G12D/p53flox/+ mouse treated with adenovirus-delivered Cre-recombinase. Cells were grown on collagen-coated tissue culture flasks for < 10 passages.
	KPC-2-mCherry (Jiang et al., 2016) cell line was derived from pancreatic tumors of a 6-month-old female p48-CRE+/LSL-KRASG12D/p53flox/+ mouse, and tumor cells additionally were modified to express mCherry and click beetle red luciferase.

Authentication	Cell lines were characterized for epithelial origin for the presence of EpCAM and absence of vimentin and CD45 in pancreatic tumor cell lines. Pancreatic tumor cell lines also underwent full exome sequencing to validate C57BL/6J identity.
Mycoplasma contamination	All cell lines tested negative for mycoplasma comtamination before in vivo implantation into mice.
Commonly misidentified lines (See ICLAC register)	No commonly misidentified lines were used.

Animals and other research organisms

Policy information about studies involving animals; ARRIVE guidelines recommended for reporting animal research, and Sex and Gender in Research

Laboratory animals	The following mouse strains (Mus musculus) were used as part of this study: C57BL/6J mice Jackson Laboratory Cat#000664 FVB/NJ mice Jackson Laboratory Cat#001800 CCR2 knockout mice (C57BL/6J background) Jackson Laboratory Cat# 004999 CSF1R-mer-iCre-mer mice (FVB/NJ background)Jackson Laboratory Cat# 019098 Rosa26-LSL-tdTomato mice (FVB/NJ background)Laboratory of Gregory Longmore N/A Flt3-Cre mice (C57BL/6J background) Laboratory of Thomas Boehm N/A Rosa26-eYFP (C57BL/6J background) mice Jackson Laboratory Cat#006148 CX3CR1-CreERT2 (C57BL/6J background) mice Jackson Laboratory Cat#025524 CX3CR1-GFP mice (C57BL/6J background) Jackson Laboratory Cat#005582 Lyve1-Cre mice (C57BL/6J background) Laboratory of Gwendalyn Randolph N/A CSF1R-flox mice (C57BL/6J background) Laboratory of Gwendalyn Randolph N/A p48-Cre;ROSA26-rtTa-IRES-EGFP;TetO-KRASG12D (iKRAS*) mice Laboratory of Marina pasca di Magliano N/A p48-Cre mice (C57BL/6J background) Laboratory of Sunil Hingorani N/A LSL-KrasG12D mice (C57BL/6J background) Jackson Laboratory Cat#008179 p53fl/fl mice (C57BL/6J background) Jackson Laboratory Cat#008462
Wild animals	No wild animals were used.
Reporting on sex	For all mouse experiments, cohorts were of equal numbers of each sex (both male and female) when possible. For experiments using Flt3-Cre;LSL-YFP mice, only male mice were used as the Flt3-Cre gene is present on the Y chromosome. None of the findings appear to apply to only one sex.
Field-collected samples	No field-collected samples were used.
Ethics oversight	All animal studies were completed in accordance with NIH-AALAC standards and consistent with Washington University School of Medicine IACUC regulations (protocol #19-0856), and studies were approved by Washington University School of Medicine Institutional Animal Studies Committee. All animals were housed in barrier facility under 12-hour light/dark cycle with 1-5 mice per cage.

Note that full information on the approval of the study protocol must also be provided in the manuscript.

Clinical data

Policy information about clinical studies
All manuscripts should comply with the ICMJE guidelines for publication of clinical research and a completed CONSORT checklist must be included with all submissions.

Clinical trial registration	*Provide the trial registration number from ClinicalTrials.gov or an equivalent agency.*
Study protocol	*Note where the full trial protocol can be accessed OR if not available, explain why.*
Data collection	*Describe the settings and locales of data collection, noting the time periods of recruitment and data collection.*
Outcomes	*Describe how you pre-defined primary and secondary outcome measures and how you assessed these measures.*

Flow Cytometry

Plots

Confirm that:

☒ The axis labels state the marker and fluorochrome used (e.g. CD4-FITC).

☒ The axis scales are clearly visible. Include numbers along axes only for bottom left plot of group (a 'group' is an analysis of identical markers).

☒ All plots are contour plots with outliers or pseudocolor plots.

☒ A numerical value for number of cells or percentage (with statistics) is provided.

Methodology

Sample preparation	Mice were sacrificed by cardiac perfusion with ~10-15mL PBS-heparin under isofluorane anesthesia. Pancreas or tumor tissue was then isolated, minced with scissors, and digested in ~15-25mL Dulbecco's Modified Eagle Medium (DMEM) with 2mg/mL Collagenase A and 1x DNase I for either 15 minutes (steady-state pancreas and cerulein treated pancreas) or 25 minutes (tumor tissue) at 37°C with constant stirring. Digestion buffer was quenched with 3mL fetal bovine serum (FBS) and filtered through 100uM Nylon mesh, pelleted by centrifugation (2000rmp for 5 min) and resuspended in FACS buffer (1% BSA in PBS). Brain tissue was minced and triturated through 40uM Nylon mesh and resuspended in FACS buffer to obtain single-cell suspension. Cell suspensions were then blocked with rat anti-mouse CD16/CD32 antibodies for 10 minutes on ice, pelleted by centrifugation, and stained with fluorophore-conjugated extracellular antibodies for 25 minutes on ice. For samples with endogenous fluorescent protein labeling, cells were then washed twice with FACS Buffer, then run on BD Fortessa X20 immediately. For unlabeled cells, samples were washed twice following antibody staining, fixed with BD Fixation Buffer for 30 minutes on ice, washed, and resuspended in FACS Buffer. Fixed samples were stored at 4°C and run on BD Fortessa X20 within two weeks. For samples requiring intracellular staining, cells were washed following extracellular staining, and stained using eBioscience FoxP3 Transcription Factor Staining Kit according to instructions by manufacturer. To quantify proliferating cells in Flt3-YFP mice, tissue was digested and extracellular staining was conducted as described above. Cells were then fixed in 4% paraformaldehyde for 10 minutes on ice, then permeabilized in ice-cold 70% ethanol for 3 hours, and stained with Ki-67 antibody diluted in FACS Buffer for 20 minutes on ice. Cells were then washed twice and immediately run on BD Fortessa X20. To quantitate blood monocytes, 100uL blood was obtained by cardiac puncture prior to perfusions and deposited into PBS-heparin. Blood was then pelleted by centrifugation, resuspended in 5mL red blood cell lysis buffer for 10 minutes at room temperature, cells pelleted by centrifugation, then stained with fluorophore-conjugated antibodies for 25 minutes on ice. Cells were then fixed in BD Fixation Buffer for 30 minutes on ice, washed twice with FACS Buffer, and stored at 4°C and run on BD Fortessa X20 within two weeks. For experiments requiring blood quantitation prior to mice being sacrificed, blood was obtained by tail vein bleeding, resuspended in RBC Lysis Buffer, stained with extracellular antibodies as described above.
Instrument	BD Fortessa X20, BD Aria-II
Software	BD FACSDiva software was used for acquiring all data. FlowJo software (FlowJo LLC) was used for analysis of all flow cytometry data.
Cell population abundance	For sorted cells for single-cell RNA-sequencing, abundance and purity were determined after clustering cells and identifying cell populations. Common cell type specific markers (CSF1R, C1QA, C1QB) were used to identify macrophage clusters and remove contaminants.
Gating strategy	Relevant gating strategies are provided in Extended data figures 1A and 8D. For pancreas macrophages, cells were gated on singlets, CD45+, CD11b+, CD3- and CD19-, Ly6C-, Ly6G-, F4/80+ and MHCII-hi and MHCII-lo. For pancreas fibroblasts, cells were gated on singlets, CD45-, EpCAM- and CD31-, Keratin-, Podoplanin+ and PDGFRa-hi/lo, aSMA+ for myFibs, Ly6C+ for iFibs, or Ly6C- and SMA- then MHCII+ for apFibs, and PDGFRa+.

☒ Tick this box to confirm that a figure exemplifying the gating strategy is provided in the Supplementary Information.